



Post-Variscan thermal history of the Moravo-Silesian lower Carboniferous Culm Basin (NE Czech Republic - SW Poland)

Dariusz Botor ^{a,*}, István Dunkl ^b, Aneta Anczkiewicz ^c, Stanisław Mazur ^c

^a AGH University of Science and Technology, Faculty of Geology, Geophysics and Environmental Protection, 30-059 Kraków, al. Mickiewicza 30, Poland

^b Department of Sedimentology and Environmental Geology, Geoscience Centre, University of Göttingen, Goldschmidtstrasse 3, Göttingen D-37077, Germany

^c Institute of Geological Sciences PAS, 31-002 Kraków, Sienacka 1, Poland



ARTICLE INFO

Article history:

Received 22 December 2016

Received in revised form 26 June 2017

Accepted 28 June 2017

Available online 30 June 2017

Keywords:

Thermochronology

Zircon

Apatite

Moravo-Silesian Culm Basin

Rheno-Hercynian Zone

Variscides

ABSTRACT

Apatite fission track analysis (AFT) and zircon (U-Th)/He thermochronology (ZHe) have been carried out for a lower Carboniferous greywacke succession of the Moravo-Silesian Culm Basin in the Nízký Jeseník Mountains. The range of apparent zircon helium ages is 303–233 Ma (late Carboniferous to Early Triassic) in the eastern part of the basin, whilst they are significantly younger in the western part, ranging from 194 to 163 Ma (Early-Middle Jurassic). Apatite fission track central ages range from 152 (Latest Jurassic) to 44 Ma (Eocene), with the majority being grouped between 114 (Aptian) and 57 Ma (Paleocene). All samples experienced substantial post-depositional thermal reset; both the AFT ages and the ZHe are considerably younger than the depositional ages. The mean track length varies in the range between 12.5 and 15.4 µm. The unimodal track length distribution, the relatively short mean track length (in most samples), and their rather low standard deviation values (1.2 to 2.1 µm) indicate that their thermal history was determined by Variscan and post-Variscan heating event(s) followed by a prolonged residence in the apatite partial annealing zone in the Mesozoic and finally by cooling in the Paleogene. Geological evidence combined with thermal modeling based on AFT and ZHe data indicate that the lower Carboniferous strata had already reached maximum palaeotemperatures in the late Carboniferous, however, they were presumably later re-heated during the Permian-Triassic. Post-Variscan extensional tectonics events were responsible for high heat flow that together with Carboniferous burial could account for the reset of both thermochronometers. A major phase of cooling occurred in the Late Cretaceous. Finally, exhumation was probably faster in the Paleogene, causing the present-day exposure of the studied rocks.

© 2016 Elsevier B.V. All rights reserved.

1. Introduction

The Moravo-Silesian Zone (MSZ) is located in the eastern part of the Czech Republic and south-western Poland, at the eastern margin of the Bohemian Massif (Fig. 1). MSZ is often considered the eastward continuation of the Rheno-Hercynian Zone of the European Variscides (e.g., Dvořák and Paproth, 1969; Franke, 1995; McCann et al., 2006; Kröner et al., 2008). The lower Carboniferous Moravo-Silesian Culm Basin, being part of the MSZ, represents the outcrop of the Variscan foreland basin that was deformed and partly included in an orogenic accretionary wedge (Čížek and Tomek, 1991; Dvořák, 1994; Kumpera and Martinec, 1995; Kalvoda et al., 2008).

The orogenic evolution of the MSZ is relatively well constrained by high-temperature geochronometers (e.g., Schulmann et al., 1991; Štípká and Schulmann, 1995; Schulmann and Gayer, 2000; Schulmann et al., 2005; Jastrzębski et al., 2013). However, its low-

temperature, post-orogenic history is still a matter of debate, particularly due to the sparsely preserved post-Carboniferous geological record (Maluski et al., 1995; Danišk et al., 2012; Sobczyk et al., 2015; Botor et al., 2017). Previous low-temperature studies in the Bohemian Massif and adjacent areas were mostly based on AFT data. They identified several cooling events throughout the Mesozoic and Cenozoic (Wagner et al., 1997; Hejl et al., 1997, 2003; Coyle et al., 1997; Thomson and Zeh, 2000; Glasmacher et al., 2002; Ventura and Lisker, 2003; Aramowicz et al., 2006; Martinek et al., 2006; Filip et al., 2007; Ventura et al., 2009; Vamvaka et al., 2014). However, Danišk et al. (2012) and Sobczyk et al. (2015) proposed significant sedimentary burial during the Late Cretaceous that caused resetting of ZHe ages in the middle part of the Sudetes. These studies suggest that the Bohemian Massif experienced a complex post-orogenic thermal evolution that may have been influenced by various processes: burial under Mesozoic sediments, Late Cretaceous exhumation related to far field compression from the Alpine Orogen and/or reheating and exhumation related to Mesozoic extensional tectonics and the opening of the European Cenozoic Rift System in the Eocene-Oligocene. The aim of this study is to fill the gap in understanding of the regional thermal history by employing fission-track and helium

* Corresponding author.

E-mail addresses: botor@agh.edu.pl (D. Botor), istvan.dunkl@geo.uni-goettingen.de (I. Dunkl), ndstruzi@cyf-kr.edu.pl (A. Anczkiewicz), ndmazur@cyf-kr.edu.pl (S. Mazur).

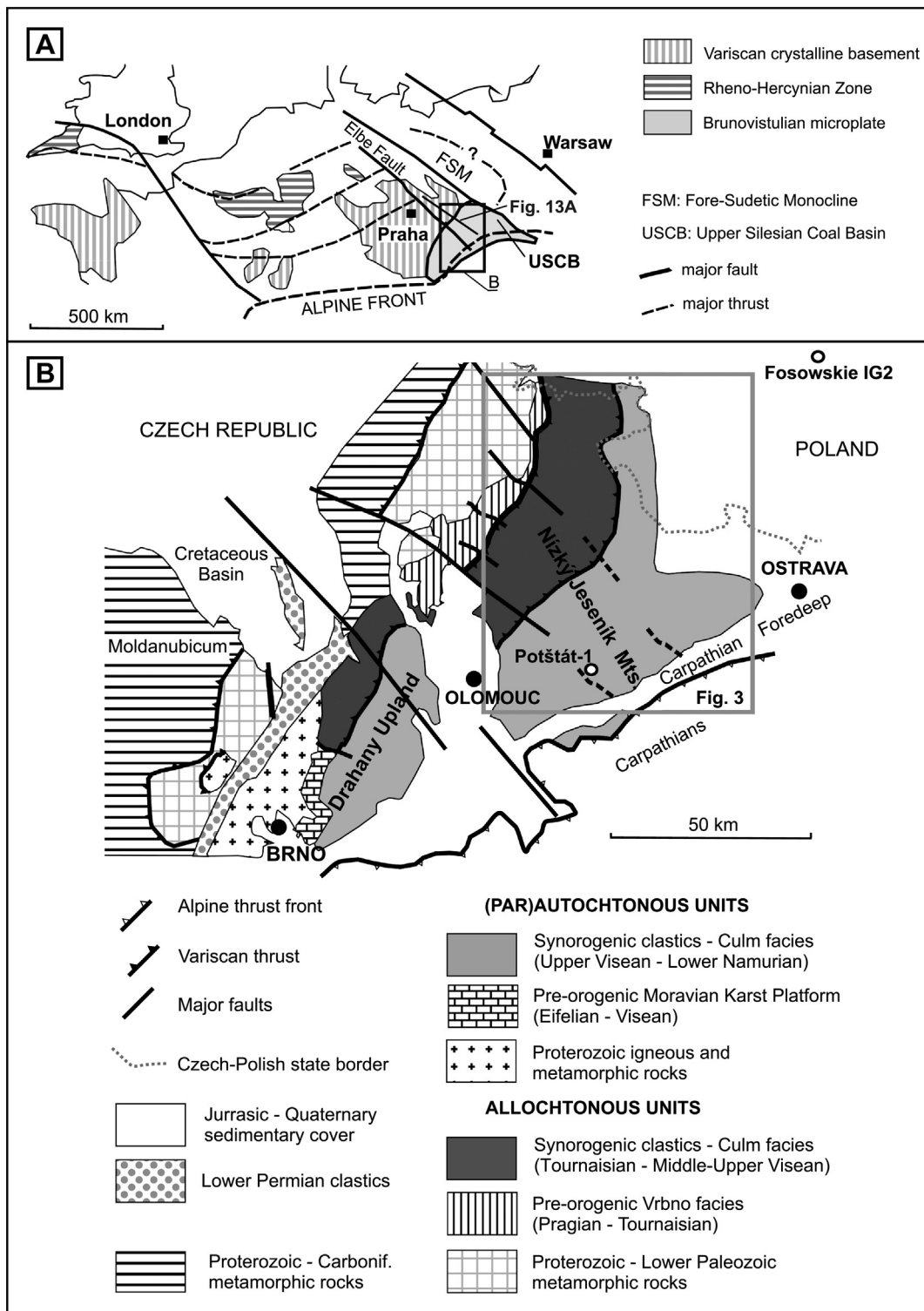


Fig. 1. A: Position of the study area in the European Variscides. B: Simplified geological map of the study area (based on Unrug, 1977; Unrug and Dembowski, 1971; Dvořák, 1989; Kumpera and Martinec, 1995; Kalvoda et al., 2008).

thermochronology to constrain the late and post-Variscan thermal history of the eastern margin of the Bohemian Massif in the Moravo-Silesian Culm Basin (MSCB), where no such data exist so far.

2. Geological setting

The Moravo-Silesian Fold-and-Thrust Belt (MSFTB; Mazur et al., 2006) represents the western, highly deformed allochthonous part of

the MSCB that extends in the N-S direction along the NE margin of the Bohemian Massif (Fig. 1; Dvořák and Paproth, 1969; Unrug and Dembowski, 1971; Schulmann et al., 1991; Franke, 1995; Fritz and Neubauer, 1995; Schulmann and Gayer, 2000; Franke and Želaźniewicz, 2000). The MSFTB corresponds to the eastern part of the Moravo-Silesian Zone (Dallmeyer et al., 1992; Franke and Želaźniewicz, 2000; Hartley and Otava, 2001; Mazur et al., 2006) and it is composed of unmetamorphosed to slightly metamorphosed

Cambrian to upper Carboniferous sediments and volcanics (Kalvoda et al., 2008). Towards the E, the heavily deformed MSFTB grades into the less deformed MSCB that is elongated SW–NE to SSW–NNE, parallel to the overall structural trend in the eastern part of the MSZ (Fig. 1; Schulmann et al., 1991; Fritz and Neubauer, 1995). The structure of the MSFTB is interpreted as a thin-skinned accretionary wedge composed of superficial flysch nappes, thrust over the parautochthonous MSCB, the Neoproterozoic crystalline basement of the Brunovistulian Terrane and its pre-orogenic Devonian sedimentary cover (Fig. 2; Dudek, 1980; Kalvoda et al., 2008). The thrusting took place during the late phases of Variscan plate convergence (330–310 Ma; late Carboniferous) under a compressive to right-lateral transpressive tectonic regime (Schulmann and Gayer, 2000). In the MSZ the intensity of deformation, metamorphism and the sediment composition changes in the W–E to NW–SE directions, perpendicular to Variscan structural grain (Rajlich, 1990; Chadima et al., 2006; Bábek et al., 2005, 2006, 2008). Prominent regional fault systems with NE–SW and NW–SE directions were developed as a result of Variscan tectonics (Rajlich, 1990; Schulmann et al., 1991; Chadima et al., 2006; Kalvoda et al., 2008).

The Culm sediments represent a lower Carboniferous foreland basin that was developed in front of the crystalline nappes of the MSZ and partly incorporated into an accretionary wedge as the MSFTB. Deep-water synorogenic siliciclastics of the Culm basin include conglomerates, greywackes, sandstones, siltstones and mudstones. They were deposited from turbidity currents and sandy and cohesive debris flows.

They are exposed in the Drahany and the Nízký Jeseník Culm sub-basins separated by the Elbe lineament (Fig. 1) (Kumpera, 1983; Hartley and Otava, 2001; Kumpera and Martinec, 1995; Bábek et al., 2004). Two major tectonic units are distinguished: (1) an allochthonous unit including Andělská Hora, Horní Benešov, Protivanov and partly Rozstání Formations, and (2) a parautochthonous unit comprising Moravice, Hradec–Kyjovice, Myslejovice and partly Rozstání Formations (Zapletal et al., 1989; Cháb et al., 1990; Kumpera and Martinec, 1995; Grygar and Vavro, 1995; Čížek and Tomek, 1991; Bábek et al., 2006). The Drahany subbasin represents a proximal and the Nízký Jeseník sub-basin a distal section of the formerly continuous MSCB (Kumpera and Martinec, 1995; Hartley and Otava, 2001).

The lower Carboniferous Culm sequence is 4.7 to 7.5 km thick (Kumpera, 1983; Kumpera and Martinec, 1995; Hartley and Otava, 2001; Mazur et al., 2006). To the E, the Culm siliciclastics are overlain by Namurian to Westphalian paralic and continental coal-bearing sediments of the Upper Silesian Coal Basin, representing the final depositional phase in the evolution of the Moravo–Silesian Basin (Kotas et al., 1983; Kalvoda et al., 2008). The age of the synorogenic siliciclastics in the Culm basin (Fig. 2) is early Viséan to the earliest Namurian (Dvořák, 1973; Kumpera, 1983; Zapletal et al., 1989; Dvořák, 1994; Kalvoda et al., 2008; Jirásek et al., 2014). The lithostratigraphic subdivision of sediments in the MSCB of the Nízký Jeseník Mts. is summarized in Fig. 2.

The MSCB was subjected to diachronous inversion after the early Namurian, resulting in a gradual eastward decrease in the age and

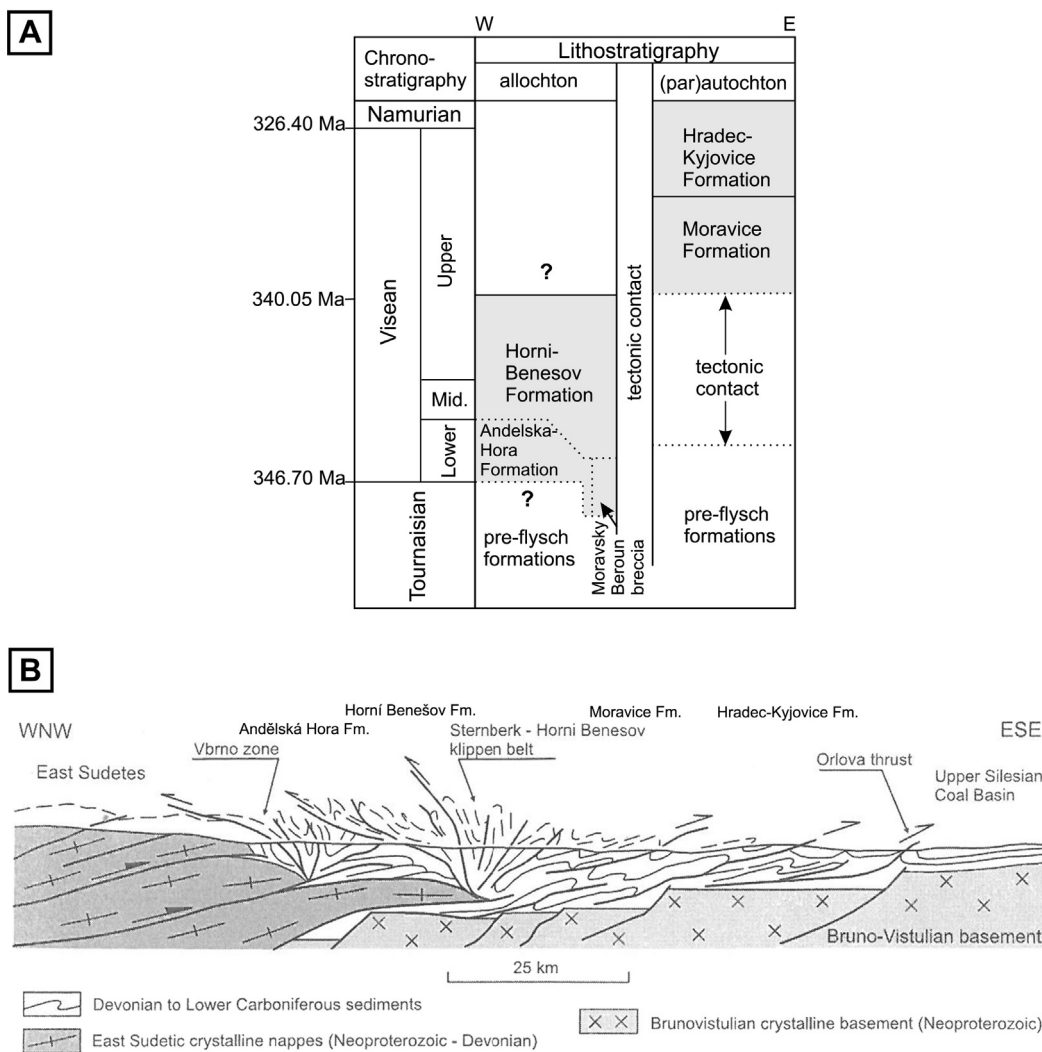


Fig. 2. A: Stratigraphy of the Moravo-Silesian Culm Basin in the Nízký Jeseník Mts. (based on Kumpera, 1983; Zapletal et al., 1989; Dvořák, 1989; Kalvoda et al., 2008; Jirásek et al., 2014). B: Simplified geological cross-section across the Moravo-Silesian fold-and-thrust belt (based on Grygar and Vavro, 1995; Kröner et al., 2008).

intensity of deformation (Kumpera and Martinec, 1995). The inversion of the eastern part of the basin was related to the formation of an imbricate thrust system of eastern polarity (Rajlich, 1990). At the same time, the western part of the basin was thrust westwards (i.e., it underwent backthrusting) onto the metamorphosed Devonian succession of the east-vergent MSZ nappe complex (Fig. 2B; Cháb, 1990; Čížek and Tomek, 1991; Kröner et al., 2008). In this way, basin inversion resulted in the development of a divergent geometry of the MSFTB (Kröner et al., 2008). The axial part of the belt contains Devonian-age rocks, upthrown along high-angle, regional shear zones as a major pop-up structure (Kumpera and Martinec, 1995; Schulmann and Gayer, 2000). The western, marginal part of the MSFTB was initially overlain by crystalline thrust sheets of the MSZ before the main phase of basin inversion. As a result of tectonic thickening of their overburden, the Carboniferous complexes in this part of the basin suffered lower greenschist facies metamorphism (Cháb, 1990) and acquired a structural pattern analogous to that of the allochthonous Devonian Vrbno group (Fig. 2B; Kröner et al., 2008). The low grade metamorphosed Culm rocks contain a NNE–SSW trending, steeply dipping foliation and a stretching lineation plunging to the N or NE at a shallow angle (Kröner et al., 2008). The age of deformation presumably corresponds to the cooling of Devonian rocks in this area, which was determined by the Ar/Ar method at c. 300 Ma (Maluski et al., 1995).

2.1. Variscan evolution

A tectonic load induced by the emplacement of Variscan nappes resulted in flexural subsidence of the western margin of the Brunovistulian microplate and deposition of synorogenic, deep-marine early Viséan to earliest Namurian siliciclastics – Culm facies (Dvořák, 1973; Kumpera, 1983; Špaček and Kalvoda, 2000; Zapletal et al., 1989). In the late Viséan times, the basin started to become overfilled (Hartley and Otava, 2001; Bábek et al., 2004), which eventually led to cessation of the deep-marine deposition and beginning of shallow-marine and continental sedimentation in the early Namurian. The synorogenic flysch facies pass gradually upward into Namurian to Westfalian paralic and continental coal-bearing molasse of the Upper Silesian Coal Basin (Kalvoda et al., 2008). During the late phases of plate convergence, a compressive tectonic regime was replaced by dextral transpression that overprinted the MSZ but left the weaker deformed MSCB mostly untouched (Rajlich, 1990; Schulmann and Gayer, 2000).

2.2. Post-Variscan evolution

Late stages of Variscan convergence in the MSZ were characterized by rapid tectonic inversion and exhumation of the consolidated Paleozoic sequences. This is documented by c. 310–290 Ma amphibole and mica Ar/Ar cooling ages (Maluski et al., 1995; Schneider et al., 2006) and it can also be inferred from the thick (up to 3 km), coarsening-upward sequence of late Paleozoic sediments in the adjacent foreland and intramontane basins, which point to an increase in relief (Malkovský, 1987; Mazur et al., 2006, 2010). In the Sudetes Mts. fine-grained sandstones, siltstones, calcareous and gypsum horizons of late Permian-Early Triassic age are interpreted as an indication of the peneplanation of the Sudetic basement blocks (Lorenz and Mroczkowski, 1978; Malkovský, 1987; Feist-Burkhardt et al., 2008; Wojewoda et al., 2016). Their thickness is <150–200 m. Between the Middle Triassic and Middle Jurassic, the Bohemian Massif formed a large and coherent high (Ziegler and Dèzes, 2007). No sediments of the Middle Triassic to Early Cretaceous age are known in the area, with the exception of a few tens of meters thick Middle-Upper Jurassic limestone found in the southern and northern part of the Bohemian Massif (Eliáš, 1981; Malkovský, 1987; Adámek, 2005). The Jurassic transgression was followed by a period of continental erosion/non-deposition that is represented by a stratigraphic gap and absence of sediments. The possible original thickness of the late Permian to Late

Jurassic sediments was comparatively low (<300 m) and was further reduced by penecontemporaneous weathering, chemical denudation and erosion (Eliáš, 1981; Malkovský, 1987; Adámek, 2005). Therefore, the late Permian to Late Jurassic sedimentary cover had no influence on the thermal history of Carboniferous rocks in the study area.

During Cenomanian, a transgression covered again large parts of the Bohemian Massif. A system of rapidly subsiding basins formed along reactivated Variscan shear zones of the Elbe Fault System during dextral transtension and at least ~1000 m of shallow marine sediments were deposited in the northern Bohemian Massif (Skoček and Valečka, 1983; Uličný, 2001; Scheck et al., 2002; Uličný et al., 2009; Wojewoda et al., 2016). Paleogeographic reconstructions gave rise to the often-putulated interpretation that the Bohemian Cretaceous Basin was surrounded by an archipelago of emerged paleo-highs from which the nearshore siliciclastic sediments were derived (Skoček and Valečka, 1983; Milewicz, 1997; Uličný, 2001). The extent of these assumed islands is a matter of controversy as the amount of eroded Cretaceous strata has not been quantified and the provenance data do not support such paleogeographic reconstructions (Danišík et al., 2012; Biernacka and Józefiak, 2009).

In the late Turonian to Paleocene, the Bohemian Massif was affected by transpressional deformation induced by far-field stresses from the Europe-Africa plate convergence (Kley and Voigt, 2008). This led to reactivation of the NW-SE striking Variscan basement grain within the Elbe Fault System with vertical offsets of several kilometers (Scheck et al., 2002), formation of thrust-related uplifts, erosion of elevated basement blocks and inversion of the Cretaceous basins (Kley and Voigt, 2008). This is evidenced by deformation of the Cretaceous strata, the abrupt cessation of sedimentation in the Late Cretaceous intramontane basins and also by a distinct cooling phase recorded by thermochronological data in the western and central parts of the Sudetes (Skoček and Valečka, 1983; Jarząbowski-Szulc, 1984; Jarząbowski-Szulc et al., 2009; Ziegler, 1987; Wojewoda, 1997; Uličný, 2001; Aramowicz et al., 2006; Ventura et al., 2009; Danišík et al., 2010; Sobczyk et al., 2015; Wojewoda et al., 2016).

Subsequently, the Bohemian Massif was subjected to profound weathering and erosion, resulting in the development of a peneplain on which thin Late Eocene to Oligocene fluvial and lacustrine clastics were locally deposited. East and southeast of the Bohemian Massif, transgressive late Eocene and Miocene marine series of the evolving Alpine-Carpathian flexural foreland basin were deposited (Demek, 1975; Jahn, 1980; Ziegler, 1987; Ziegler and Dèzes, 2007; Migoń and Lidmar-Bergström, 2001). In the late Eocene, a SW-NE trending Eger rift associated with alkaline volcanism developed as part of the central European Cenozoic Rift System in the NW part of the Bohemian Massif (Dèzes et al., 2004). During the Neogene, differential subsidence, resulting in continental coal-bearing sedimentation in the Sudetic region, commenced (Dyjor, 1986; Kasiński and Panasiuk, 1987). Oligocene-Miocene and Pliocene basaltic volcanism penetrated the Sudetes and adjacent areas (Birkenmajer et al., 1977, 2002a, b, 2004; Badura et al., 2005; Ulrych et al., 2011). Mid-Miocene to recent uplift and deformation of the Bohemian Massif can be attributed to lithospheric buckling and transpressional reactivation of preexisting crustal discontinuities in response to the Neogene progressive build-up of intraplate compressional stresses that reflect increasing collisional coupling between the East-Alpine-Carpathian orogenic wedge and its northern foreland (Ziegler et al., 2002; Ziegler and Dèzes, 2007).

2.3. Previous studies related to the thermal evolution of the MSCB

2.3.1. Organic maturity and clay mineral data

The thermal history of the MSCB was investigated by means of random vitrinite reflectance (VR) and maximum vitrinite reflectance (R_{max}) (Dvořák and Wolf, 1979; Dvořák, 1989; Franců et al., 1999, 2002; Nowak, 2003), illite “crystallinity” (Dvořák, 1989; Franců et al., 1999) and the Conodont Alternation Index (CAI) methods (Bábek et

al., 2008). The observations that were recently summarized by Botor et al. (2017). In the SE part of the Drahany Upland, the illite “crystallinity” values range from 0.44 to 1.46 $\Delta^2\Theta$, the VR from 1.1 to 2.2%, whereas CAI oscillates around 3. Towards the west and northwest, organic and clay mineral indices increase. In the NW part of the Drahany Upland, the illite “crystallinity” ranges from 0.24 to 0.36 $\Delta^2\Theta$, VR from 3.2 to 5.2%, and CAI is in the range of 4–5 (Dvořák and Wolf, 1979; Dvořák, 1989; Franců et al., 1999, 2002; Bábek and Franců, 2004; Bábek et al., 2006, 2008). In the eastern Nízký Jeseník, the R_{max} values are in the range of 0.5 to 2.8% in Carboniferous strata, and towards the west reach 4–6% on the surface (Dvořák, 1989). Locally, values as high as 9% R_{max} were measured (Dvořák and Wolf, 1979; Dvořák, 1989). Taking into account all vitrinite reflectance, Raman spectroscopy and clay mineral data available in the Nízký Jeseník area (Dvořák and Wolf, 1979; Dvořák, 1989; Nowak, 2003; Bábek et al., 2008; Botor et al., 2017), the estimated maximum paleotemperature increases from the east (~180–200 °C) to the centre (~200–330 °C) and west (~300–350 °C) of the MSCB (Fig. 3).

In the MSCB, the intensity of thermal alteration decreases upwards in the stratigraphic sequence, i.e., from the west to the east, showing a burial-related trend (Franců et al., 2002). The distribution of vitrinite reflectance and illite “crystallinity” was interpreted by the model of deep, mainly tectonically driven burial with lower heat flow in the western hinterland and relatively shallower burial with equal or slightly higher heat flow in the eastern foreland basin (Franců et al., 1999, 2002). However, in some wells the maturity data do not show any significant depth-related trend. In the Potštát-1 well, a saw-tooth down-hole pattern of R_{min} and R_{max} values indicates that Variscan thrust tectonics, which is also visible in seismic data, did not affect the area before it attained its final thermal maturity (Bábek et al., 2005). This suggests a possible influence of penetrating hydrothermal fluids or localized deformation. The organic maturity data distribution indicates that especially in the western part of the study area the isotherms intersect major Variscan tectonic structures (Bábek et al., 2005). Recently, Botor et al. (2017) based on Raman spectroscopy and vitrinite reflectance data have postulated that the western part of the MSCB was re-heated due to fluid

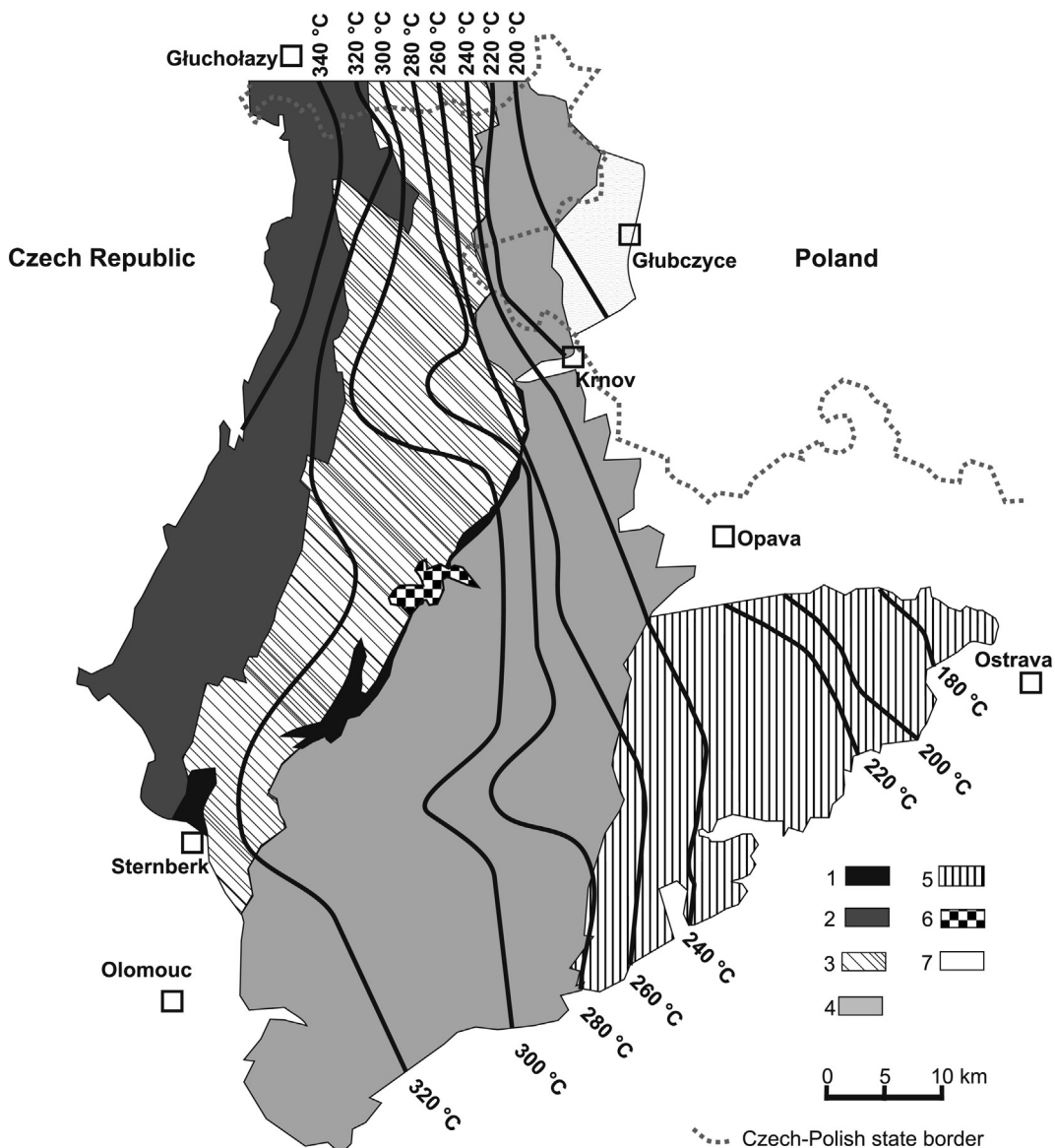


Fig. 3. Paleotemperature distribution based on vitrinite reflectance and Raman spectroscopy data (Botor et al., 2017), illite crystallinity (Dvořák, 1989) and Conodont Alteration Index (Bábek et al., 2008) shown on the background of geological map of the Moravo-Silesian Culm Basin (geological map modified based on Dvořák, 1989, 1994; Kumpera and Martinec, 1995). 1 - preflysch beds (Sternberk-Horní Benešov Zone), 2 - Andělská Hora Formation, 3 - Horní Benešov Formation, 4 - Moravice Formation, 5 - Hradec-Kyjovice Formation, 6 - Neovolcanics rocks, 7 - Neogene sedimentary rocks.

circulation probably in the Permian-Triassic time span. The Jurassic-Miocene burial did not alter the maturity pattern (Bábek et al., 2005), the observation that is also confirmed by low vitrinite reflectance values from Carboniferous strata under the cover of the Carpathians and the Carpathian Foredeep (Dvořák, 1989; Francú et al., 1999). Therefore, the peak temperatures must have been reached before the Jurassic.

2.3.2. Hydrothermal veins

Numerous hydrothermal veins occur in the MSCB, providing record of fluid penetration into the Carboniferous rocks. Several historical mining districts are concentrated on sites of mineralization, where mainly silver and lead but also gold were mined (Losert, 1957; Zimák et al., 2002; Kučera et al., 2010; Dolníček et al., 2014). Common ore minerals are galena, sphalerite, chalcopyrite, pyrite and marcasite, whilst quartz and carbonates represent the main gangue minerals. The veins have mostly massive, brecciated, deformational and drusy structures, their thickness ranges between few mm and 0.5 m (Zimák et al., 2002; Kučera and Slobodník, 2002; Dolníček et al., 2014). The age of the vein formation is uncertain. Kučera and Slobodník (2002) argued that these veins fill the extensional structures oriented perpendicularly to the bedding planes and their origin is post-Variscan and possibly related to Alpine compression. Indeed, a regional distribution of hydrothermal mineralization points to more extensive migration of fluids along fractures formed in a regional stress field, perhaps during Alpine (Slobodník et al., 2001) or late to post-Variscan (Kříbek et al., 2009) tectonic events.

2.3.3. Thermochronological studies

The AFT studies in the Bohemian Massif and adjacent areas yielded generally Late Jurassic to Late Cretaceous apparent AFT ages (Bischoff et al., 1993; Coyle et al., 1997; Hejl et al., 1997, 2003; Vamvaka et al., 2014). The Ruhla Crystalline Complex and the Thuringian Forest reveal cooling during the Late Cretaceous (Thomson and Zeh, 2000; Thomson, 2001). Along the NW margins of the Bohemian Massif (Erzgebirge and West Sudetes), AFT data demonstrate cooling during the Jurassic and/or Cretaceous (Ventura and Lisker, 2003; Lange et al., 2008; Ventura et al., 2009; Voigt, 2009; Danišík et al., 2010, 2012; Wolff et al., 2015). In the Erzgebirge and the Góry Sowie Massif, a phase of young enhanced exhumation during the Paleogene-Neogene was also found (Ventura and Lisker, 2003; Aramowicz et al., 2006). In NE Bavaria, the AFT ages are Paleogene presumably due to a thermal overprint connected with lithospheric updoming and volcanism that are associated with the Eger Rift zone (Bischoff et al., 1993). The Late Jurassic to Late Cretaceous AFT ages in the Erzgebirge (Vamvaka et al., 2014) can be explained either by reheating of the basement rocks by the Mid-Late Jurassic and/or by Late Cretaceous marine transgression causing burial heating or by intense mid-late Mesozoic hydrothermal activity (Vamvaka et al., 2014; Wolff et al., 2015). In the NE margin of the Bohemian Massif (Sudetes Mts., but still NW from our study area) a model of Cretaceous regional burial has been recently proposed by Danišík et al. (2012) and Sobczyk et al. (2015). For the interior parts of the Bohemian Massif, e.g., the Barrandian unit, the Carboniferous to Early Jurassic AFT ages have been reported by Glasmacher et al. (2002). Hence, higher Mesozoic denudation rates are deduced from the AFT ages for the outer zones of the Bohemian Massif (Vamvaka et al., 2014). Since the Bohemian Massif consists of fault-bounded blocks separated by major lineaments (e.g., Mattern, 1995; Danišík et al., 2012) the Mesozoic AFT ages can be related to tectonic activity along these crustal discontinuities (Hejl et al., 1997; Thomson and Zeh, 2000; Ventura and Lisker, 2003). However, thermal modeling led to different scenarios for the Mesozoic to Neogene track record ranging from the increase in crustal heat flow and paleogeothermal gradients (Thomson and Zeh, 2000; Ventura and Lisker, 2003) and reburial by supracrustal rocks (Hejl et al., 2003) to gradual or slow regional denudation (Hejl et al., 1997; Glasmacher et al., 2002; Filip and Suchý, 2004). The general age pattern in the different areas of the Bohemian Massif is similar, therefore it can be assumed that

Late Jurassic to Late Cretaceous cooling is a regional feature in many marginal regions of this massif (Vamvaka et al., 2014).

3. Samples and methods

3.1. Apatite fission track dating

Apatite crystals were separated from lower Carboniferous greywacke samples collected in the Nízký Jeseník Mts. using conventional crushing, sieving, and magnetic and heavy liquids separation techniques. Apatite grains were mounted in epoxy resin on glass slides and polished to expose internal grain surfaces. Spontaneous tracks were revealed by 5 N HNO₃ at 21 °C for 20 s. Neutron fluence was monitored using CN5 uranium dosimeter glass. Thin flakes of low-U muscovite were used as external detectors. Samples together with age standards (Fish Canyon, Durango, and Mount Dromedary apatite) were irradiated with a thermal neutron nominal flux of 9×10^{15} n/cm² at the Oregon State University TRIGA reactor (USA). After irradiation, the muscovite detectors were etched in 40% HF for 45 min at 20 °C to reveal the induced tracks. For AFT analysis, we used the external detector method and the ζ age calibration method in order to determine the fission track ages (Hurford and Green, 1983; Hurford, 1990). Track counting and length measurement of horizontal confined fission tracks and the etch pit diameter (Dpar) values were carried out by means of optical microscopy at 1250× magnification using a Nikon Eclipse E-600, equipped with a motorized stage, digitizing tablet, and drawing tube controlled by program FTStage 4.04 (Dumitru, 1993). All quoted AFT ages are central ages with 1σ error (Galbraith and Laslett, 1993). The degree to which individual AFT grain ages in a sample belong to a single population was assessed by a χ^2 statistic (Galbraith, 1981). Values of P(χ^2) below 5% indicate a statistically significant spread in single grain ages and the presence of more than one population (e.g., Galbraith, 1981, 1990; Galbraith and Laslett, 1993). Crystals chosen for confined track measurements had a well-polished surface, parallel to the c-axis. For each sample, as many confined track lengths as possible were measured (Gleadlow et al., 1986). The measured confined track lengths were corrected for their crystallographic orientation by applying the computer code HeFTy to the data set (Donelick et al., 1999; Ketcham et al., 2007a). Data analyses and age calculations were based on a Zeta value ζ CN5 of 351.02 ± 7.91 for CN5 (Botor and Anczkiewicz, 2015), and accomplished by using Trackkey 4.2 software (Dunkl, 2002).

3.2. Zircon (U-Th)/He dating

Zircon crystals were handpicked following the recommendation of Farley (2002). Selected crystals were characterized by euhedral shape with two pyramidal terminations, and a width of >65 µm. The crystals were then photographed, measured for physical dimensions and loaded in Pt microtubes. The helium was extracted at ~1000 °C under high vacuum using a diode laser and measured by isotope dilution using a Hiden 3F triple-filter mass spectrometer. A “re-extract” was run after each sample to verify complete degassing of the crystals. Following degassing, samples were retrieved from the gas extraction line and spiked with calibrated ²³⁰Th and ²³³U solutions. Zircon crystals were dissolved in teflon bombs using a mixture of double distilled 48% HF and 65% HNO₃ at 220 °C for 5 days. Spiked solutions were analysed as 0.4 ml solutions by isotope dilution on a Perkin Elmer Elan DRC II ICP-MS with an APEX micro-flow nebulizer. Procedural U and Th blanks by this method are usually very stable in a measurement session and below 1.5 pg. Sm, Pt, Zr and Ca were determined by external calibration. The oxide formation rate and the PtAr - U interference was always monitored, but the effects of isobaric argides were negligible relatively to the signal of actinides. The ejection correction factors (F_t) were determined for the single crystals by a modified algorithm of Farley et al. (1996) using an in-house spreadsheet.

3.3. Thermal modeling

The modeling of the thermal history was performed by using HeFTy software (Ketcham, 2005). The program requires input data (such as measured AFT age, track length distribution, kinetic parameter as Dpar for apatite and apparent ZHe age, actinide concentration and diameter of the dated crystals) to define “acceptable” time-temperature paths that pass statistical criteria and also conform to a possible set of user-defined geological constraints (Ketcham, 2005). Thermal histories were modelled using the multi-kinetic model (Ketcham et al., 2007b). Randomly generated thermal histories predict the AFT age and length parameters, and compare them to the measured data. An acceptable fit corresponds to thermal histories representing the t-T paths that give a goodness of fit (GOF) value >0.05 for both the age and the length distribution (Ketcham, 2005). A good fit corresponds to thermal histories with a GOF value >0.5 . For a comprehensive overview of fission-track methods and their modeling techniques, see more details in Donelick et al. (2005), Ketcham (2005), and Ketcham et al. (2007b).

4. Results

4.1. Apatite fission track data

AFT analyses were performed on 27 samples. The results of the AFT analyses are presented in Tables 1–2 and Figs. 4–7. Most of the AFT central ages represent unimodal single grain age populations; except for sample 9T (Table 1, Fig. 6). Central AFT ages range from 151.6 ± 12.6 (latest Jurassic) to 43.8 ± 5.0 Ma (middle Eocene), with the majority being grouped between 113.5 (Aptian, Early Cretaceous) and 56.9 Ma (Paleocene; Table 1, Figs. 4 and 5). All the analysed samples yielded central AFT ages significantly younger than the early Carboniferous

stratigraphic age of the sediments from which they were collected (Table 1, Figs. 5 and 6). The AFT ages do not show correlation with the elevation of samples, because of small differences in elevation between the samples (<200 m). There is also no clear trend in a regional distribution of the apatite FT ages, but towards the east the AFT ages seem to be slightly older (Fig. 4).

A total of 1194 lengths of horizontal confined spontaneous fission-tracks were measured (Table 2). A mean track length (MTL) ranges from 12.5 ± 1.7 to 15.4 ± 1.5 μm (Table 2, Fig. 3); the distributions are unimodal, relatively narrow (Fig. 6). The oldest central ages, between 151 Ma and 104.2 Ma have a MTL (13.1 to 13.3 μm) lower than to the youngest (43.8 to 61.4 Ma) samples (MTL 13.5 to 15.4 μm). Nearly all samples show a negative skewness between -0.04 and -2.25 , which is a tailing towards shorter track lengths indicating simple gradual slow cooling with the exception for six samples (11M, 21S, 5B, 7B, GOL1, J1 from the central and western parts of the MSCB). The standard deviation values of track length range from 1.2 to 2.1 μm (Table 2). The measured confined track lengths were corrected for their orientation to the crystallographic c-axis by applying the HeFTy computer code to the data set (Table 2). A mean c-axis projected track length is in the range between 13.5 ± 0.31 and 15.6 ± 0.5 μm . With the exception for five samples (11M, 21S, GOL1, J1, PIE), all the samples show a negative skewness between -0.06 and -2.29 (Table 2). The standard deviation values of c-axis projected track length range from 1.0 μm to 1.9 μm (Table 2). These data indicate moderately slow cooling after a heating event(s) responsible for shortening of tracks (Green et al., 1986).

A total of 2322 Dpar values were determined for all apatite grains used in this study (Table 2). This parameter is indicative of the annealing kinetics of the apatites (Donelick et al., 2005; Ketcham et al., 2007a, 2007b). The mean Dpar values of the MSCB samples are in the range of 2.0 ± 0.3 to 2.5 ± 0.4 μm (Table 2), which generally shows

Table 1
Sample data and apatite fission-track age data.

Sample code	Sample co-ordinates	Nc	U ($\mu\text{g/g}$)	Dosimeter		Spontaneous		Induced		P (χ^2) [%]	Central age (Ma) $\pm 1\sigma$	
				ρd	Nd	ρs	Ns	ρi	Ni			
11M	49° 53.609'N	17° 42.390'E	20	29.9	12.67	3869	6.334	175	23.201	641	47.81	61.4 ± 5.6
12B	49° 47.731'N	17° 33.512'E	20	23.1	11.37	3617	8.923	209	21.175	496	90.63	84.8 ± 7.4
13D	49° 57.251'N	17° 29.896'E	15	32.6	12.27	3788	6.499	121	32.817	611	14.38	43.8 ± 5.0
14B	49° 59.492'N	17° 29.098'E	20	19.8	13.03	3869	6.070	210	18.038	624	80.82	77.7 ± 6.6
15J	49° 44.347'N	17° 26.145'E	20	24.9	12.14	3788	7.094	196	25.409	702	6.72	62.4 ± 6.2
16V	49° 53.765'N	17° 21.340'E	20	12.6	12.84	3869	5.176	157	12.957	393	98.88	90.8 ± 9.0
17S	50° 0.593'N	17° 38.308'E	20	27.8	11.65	3506	7.018	196	25.494	712	86.70	56.9 ± 4.9
18L	49° 45.350'N	17° 55.383'E	20	24.6	11.80	3506	9.859	225	23.135	528	98.75	89.0 ± 7.5
19S	49° 49.315'N	17° 54.054'E	20	14.2	12.64	3869	5.79	177	14.099	431	97.33	91.8 ± 8.6
1C	49° 45.727'N	17° 19.003'E	21	16.8	11.83	3506	5.454	190	16.794	585	67.04	70.0 ± 6.6
20R	50° 1.911'N	17° 23.807'E	24	24.1	12.04	3617	6.381	197	22.481	694	92.94	60.6 ± 5.2
21S	50° 2.519'N	17° 22.350'E	6	29.1	11.52	3617	8.492	51	25.974	156	79.84	66.8 ± 10.9
2K	50° 7.238'N	17° 37.408'E	20	20.5	13.01	3869	7.538	206	21.261	581	79.99	81.7 ± 7.0
30	49° 54.403'N	17° 17.107'E	20	17.9	12.75	3788	5.565	124	17.952	400	73.34	70.1 ± 7.5
4S	49° 41.458'N	17° 44.733'E	20	20.5	11.50	3506	6.660	146	19.934	437	93.30	68.1 ± 6.8
5B	49° 55.296'N	17° 25.208'E	20	31.5	11.68	3617	7.150	219	30.721	941	93.27	48.3 ± 3.9
6V	49° 47.593'N	17° 45.861'E	20	30.9	11.88	3506	8.254	233	29.191	824	46.44	59.6 ± 4.8
7B	49° 37.221'N	17° 39.890'E	20	24.7	12.96	3869	8.325	189	27.221	618	80.68	70.5 ± 6.3
9T	49° 44.292'N	17° 21.980'E	30	20.2	12.63	3869	6.442	325	21.546	1087	1.99	72.5 ± 6.2
BR	50° 8.490'N	17° 43.335'E	20	23.2	12.62	3869	10.424	360	23.368	807	99.29	99.5 ± 6.9
GOL1	50° 11.798'N	17° 46.989'E	26	15.7	11.78	3617	8.252	283	15.134	519	96.17	113.5 ± 9.0
GR1	50° 9.742'N	17° 40.151'E	20	18.3	11.58	3617	7.762	269	15.813	548	7.26	104.2 ± 10.2
J1	50° 17.239'N	17° 25.864'E	20	19.1	12.98	3869	5.448	178	17.844	583	78.32	70.2 ± 6.3
J3	50° 17.294'N	17° 26.417'E	20	27.2	12.81	3869	10.447	224	29.909	622	25.21	83.8 ± 7.8
KG1	50° 17.501'N	17° 24.404'E	20	25.7	11.78	3506	8.585	198	23.024	531	38.03	78.3 ± 7.3
PIE	50° 10.791'N	17° 40.341'E	20	21.6	12.74	3869	10.258	475	22.222	1029	55.09	104.0 ± 6.5
Z1	50° 7.583'N	17° 47.985'E	20	17.3	12.41	3788	11.844	276	17.079	398	94.10	151.6 ± 12.6

Nc – number of measured crystals. SD – standard deviation. Dpar is the etch pit diameter. At least four Dpar (Donelick et al., 1999, 2005) per single analysed grain have been measured. U – amount of uranium which was calculated by software Trackkey 4.2 (Dunkl, 2002). ρs – density of spontaneous tracks ($\times 106$ tracks for cm^{-2}); Ns – number of counted spontaneous tracks; ρi – density of induced tracks in external detector (mica) ($\times 106$ tracks for cm^{-2}); Ni – number of counted induced tracks; ρd – density of induced tracks in external detector which cover dosimeter (glass CN5) ($\times 106$ tracks for cm^{-2}); Nd – numbers of counted tracks. Dispersion in age is showed in % and illustrate dispersion obtained ages analyzed apatite. P (χ^2) [%] – probability homogeneity apatite population were showed by the test agreement χ^2 value (Galbraith, 1981; Green, 1981). AFT age $\pm 1\sigma$ error is a central age of sample (Galbraith and Laslett, 1993) counted by using calibration method zeta (Hurford, 1990; Hurford and Green, 1983) and dosimeter (glass) CN5. Zeta value is 356.39 ± 8.41 (A. Anczkiewicz). Lithology of all samples is greywacke.

Table 2

Detailed apatite fission-track length and Dpar data.

Sample	n CT	CT mean (μm)	CT sd (μm)	CT skew	Lc mean (μm)	Lc sd (μm)	Lc skew	n Dpar	Dpar mean (μm)	Dpar sd (μm)	Dpar skew
11M	26	14.1	1.6	0.5	14.7	1.3	0.4	80	2.3	0.3	0.1
12B	36	13.3	2.1	-1.1	14.0	1.7	-1.0	80	2.5	0.3	-0.1
13D	33	13.5	1.4	-0.1	14.2	1.3	-0.5	60	2.1	0.4	0.2
14B	40	13.5	1.5	-0.2	14.1	1.3	-0.1	81	2.4	0.4	0.3
15J	38	13.8	1.6	-0.5	14.4	1.2	-0.2	80	2.4	0.3	0.2
16V	38	14.0	1.5	-0.2	14.6	1.3	-0.4	80	2.1	0.3	0.5
17S	13	13.2	1.4	-2.2	14.0	1.0	-1.4	80	2.5	0.3	0.4
18L	44	13.2	1.6	0.0	13.9	1.3	-0.2	80	2.4	0.3	-0.3
19S	73	13.9	1.4	-0.5	14.4	1.3	-0.7	79	2.0	0.4	0.4
1C	25	13.4	1.7	-0.6	14.1	1.5	-0.9	84	2.4	0.4	-0.3
20R	109	13.9	1.5	-0.2	14.5	1.3	-0.3	221	2.0	0.4	-0.3
21S	7	15.4	1.5	0.1	15.6	1.3	0.1	24	2.3	0.3	-0.5
2K	47	13.9	1.4	-0.4	14.5	1.2	-0.8	80	2.4	0.3	0.0
30	22	12.5	1.7	-0.1	13.5	1.5	-0.5	80	2.3	0.3	0.1
4S	34	12.9	1.9	-0.5	13.7	1.5	-0.5	80	2.2	0.3	0.3
5B	60	14.0	1.4	0.1	14.6	1.2	-0.3	80	2.0	0.3	0.1
6V	30	13.0	1.3	-0.4	13.8	1.1	-1.1	80	2.2	0.4	0.2
7B	36	13.5	1.3	0.1	14.3	1.2	-0.5	80	2.1	0.4	0.1
9T	33	14.2	2.1	-1.8	14.7	1.9	-2.3	120	2.4	0.4	0.4
BR	99	13.2	1.5	-0.2	13.9	1.4	-0.7	80	2.2	0.4	0.4
GOL1	76	13.5	1.5	0.3	14.2	1.2	0.0	108	2.2	0.4	1.0
GR1	68	13.3	1.6	-0.7	14.0	1.3	-0.4	80	2.5	0.4	0.3
J1	7	13.6	1.4	1.1	14.4	1.1	0.9	80	2.3	0.3	0.1
J3	43	13.5	1.4	-1.0	14.1	1.2	-0.8	80	2.2	0.3	0.2
KG1	9	13.6	1.2	-0.4	14.0	1.1	-0.1	81	2.3	0.3	-0.3
PIE	86	13.8	1.5	-0.1	14.4	1.2	0.0	108	2.2	0.4	-0.2
Z1	62	13.1	1.2	-0.1	13.8	1.1	-0.3	76	2.1	0.3	0.1

nCT: number of measured confined tracks, CT mean: mean confined track length, std: standard deviation, skew: skewness of distribution relative to the mean value (measure of asymmetry of the distribution), Lc mean: mean track length after c-axis correction, n Dpar: number of etch pit diameters measured, Dpar mean: mean etch pit diameter.

that the analysed samples are characterized by higher resistance to annealing than typical fluoroapatites (Donelick et al., 2005; Ketcham et al., 2007a, 2007b). Nearly all samples exhibit a positive skewness between 0.04 and 1.01, with the exception for eight samples (12B, 18L, 1C, 20R, 21S, KG1, PIE, Z1). The large skewness value indicates a larger variation in etch pit size.

4.2. Zircon (U-Th)/He ages

ZHe thermochronology has been carried out on 10 samples; three or two single-crystal aliquots were dated per sample (Table 3). The spread of single grain ages within the individual samples can be related mostly to the variable zoning of actinide elements. The average ZHe ages range from 303.1 ± 15.9 to 162.9 ± 8.8 Ma (Table 3). The ZHe ages form a distinct spatial pattern, and are increasing towards the east (Fig. 4). ZHe ages from the eastern part of the study area range from 303.1 to 232.6 Ma (late Carboniferous to Early Triassic), whilst ZHe ages from the western part are significantly younger and range from 194.1 to 162.9 Ma (Early–Middle Jurassic).

4.3. Thermal modeling

In order to reconstruct thermal paths that reconcile the thermochronological data, a number of samples yielding the best quality results were chosen for thermal history modeling. The thermal modeling of samples 5B, 6V, 12B, 18L, and BR was carried out (Figs. 8 to 12) by means of the HeFTy software (Ketcham, 2005; Ketcham et al., 2007b). In the analysed sample set, the beginning of the t-T paths was defined by the estimated annual mean temperature ($\sim 25 \pm 5$ °C) during the time of deposition (~ 340 –325 Ma), whilst their end was defined by the average present-day temperature (10 °C). In this setting, calculations were performed until the software calculated 100 good paths. HeFTy models were constructed taking into account previous thermal history studies in the Bohemian Massif. A temperature value in the constrain boxes was assumed to vary from 25 to 250 °C i.e., within the range wider than sensitivity of the applied AFT and ZHe methods to avoid forcing any solutions. The ensuing five thermal history scenarios

inferred from geological constraints available (see below) are potentially plausible for the study area and they were tested by different HeFTy models (Figs. 8–12).

- (1) Permian cooling after the Variscan orogeny to the near-surface temperatures in the Early Triassic followed by thermal stagnation without any reheating until recent times. In these models, a thermal peak was in the late Carboniferous (~325–300 Ma) as suggested by Dvořák (1989) and Franců et al. (2002). Assuming such a thermal history only samples (18L and BR) from the eastern part of the MSCB yielded high GOF values (0.92–0.99) for both the ZHe and AFT data (Fig. 8). Samples from the central and western part of the MSCB yielded a worse match (samples 5B and 6V) that suggests that not only a Variscan thermal event governed their thermal history. In these models, a maximum temperature was reached in the Carboniferous (~160–250 °C) followed by a temperature decrease up to the present-day.
- (2) A Variscan thermal peak followed by cooling in the Permian and re-heating in the Triassic (Fig. 9). The Early- to Late Triassic (250–200 Ma) increase of heat flow was assumed in association with an extensional regime dominating in the NE Bohemian Massif at that time (Grygar and Vavro, 1995; Kröner and Romer, 2013; Kowalska et al., 2015). In the Triassic reheating scenarios, samples 18L and BR from the eastern part of the MSCB yielded also good GOF values (0.85–1.00). Samples 5B (GOF AFT 0.56/0.62 and ZHe 0.86) and 6V (GOF AFT 0.61/0.44 and ZHe 0.98) show poorer results, particularly for the AFT data. Sample 12B shows better results (GOF 0.83–0.97). In these models, a maximum temperature was reached in the Carboniferous by eastern samples 18L and BR (220–240 °C), whilst samples from the central and western part of study area (6V, 12B, 5B) show a maximum temperature in the Late Triassic, which was higher than the Variscan temperature (Fig. 9).
- (3) A Jurassic (200–150 Ma) thermal pulse scenario (temperature range 25–250 °C) was assumed based on the suggestion by Vamvaka et al. (2014) regarding the increase of temperature due to sedimentary burial or increased heat flow. HeFTy models

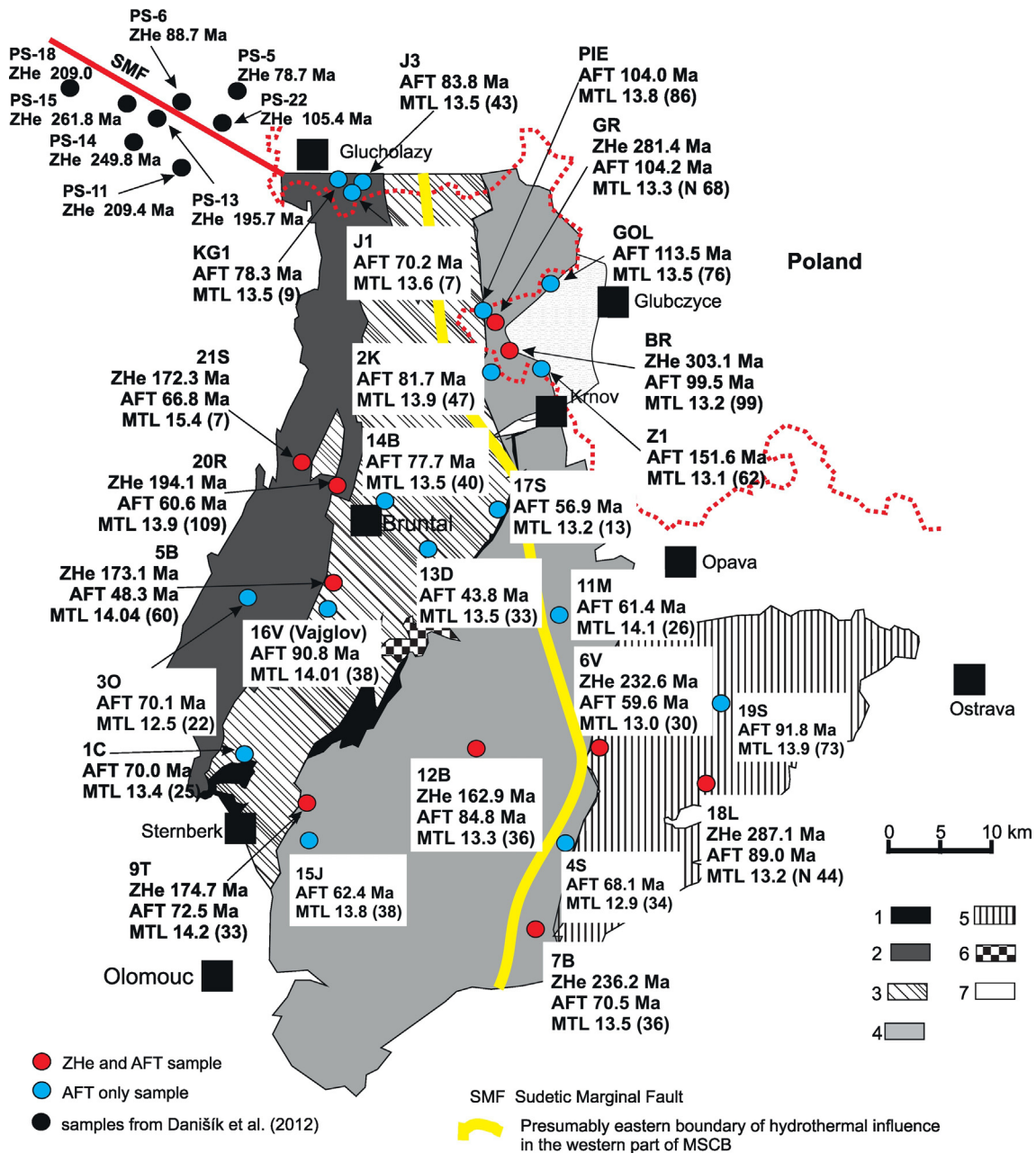


Fig. 4. Geological sketch map of the Moravo-Silesian Culm Basin showing low-T thermochronological data. ZHe: mean of zircon (U-Th)/He aliquot corrected ages, AFT: apatite fission tracks central age, MTL: mean track length. Detailed data are given in Tables 1–3. For more explanations and the names of geological units see Fig. 3.

for this scenario are shown in Fig. 10. In the 18L sample, GOF values are in the range of 0.82–0.96 showing that Jurassic re-heating was possible. The BR sample gave excellent results (GOF 0.95–0.96) showing maximum heating in the Late Jurassic. In samples 6V and 12B, GOF for the AFT data is in the range of 0.76–0.98, whilst GOF for the ZHe ages is worse (0.66–0.67). For the 5B sample the results are also good (GOF 0.86–0.91) but a significant increase in heating occurred in the Triassic instead of Jurassic, which was followed by cooling with some second-order heating events in the Paleogene-Neogene. In these models, the temperature in the Jurassic was much lower (~130–200 °C) than the Variscan temperature (~200–250 °C) (Fig. 10).

- (4) Significant Cretaceous burial (~4–6 km) of the Sudetes, as suggested by Danišk et al. (2012) and Sobczyk et al. (2015), who assumed maximum temperatures of basement during the Late

Cretaceous based on ZHe data west of our study area. With such a model, we assume that the samples were relatively close to the surface during the Early Cretaceous prior to the Late Cretaceous transgression. A constraint was set to 90–70 Ma (25–250 °C) based on the onset of sedimentation in the Cretaceous basins around the Sudetes (Skoček and Valečka, 1983; Fig. 11). Modeling of the 18L sample gave relatively poor quality results (GOF 0.65–0.81) suggesting that Cretaceous heating did not occur in this site. Modeling of the BR sample provided reasonable results (GOF 0.80–0.97). In the samples 6V and 12B, thermal history seems to be similar and GOF values are in the range of 0.80–0.97. However, the increase of temperature has started much earlier than the mid-Cretaceous. In the sample 5B, lack of good fit, low GOF for AFT length (0.18) and ZHe age (0.71), suggest a very low influence of any Cretaceous heating. In these models, a maximum temperature was reached in the Carboniferous

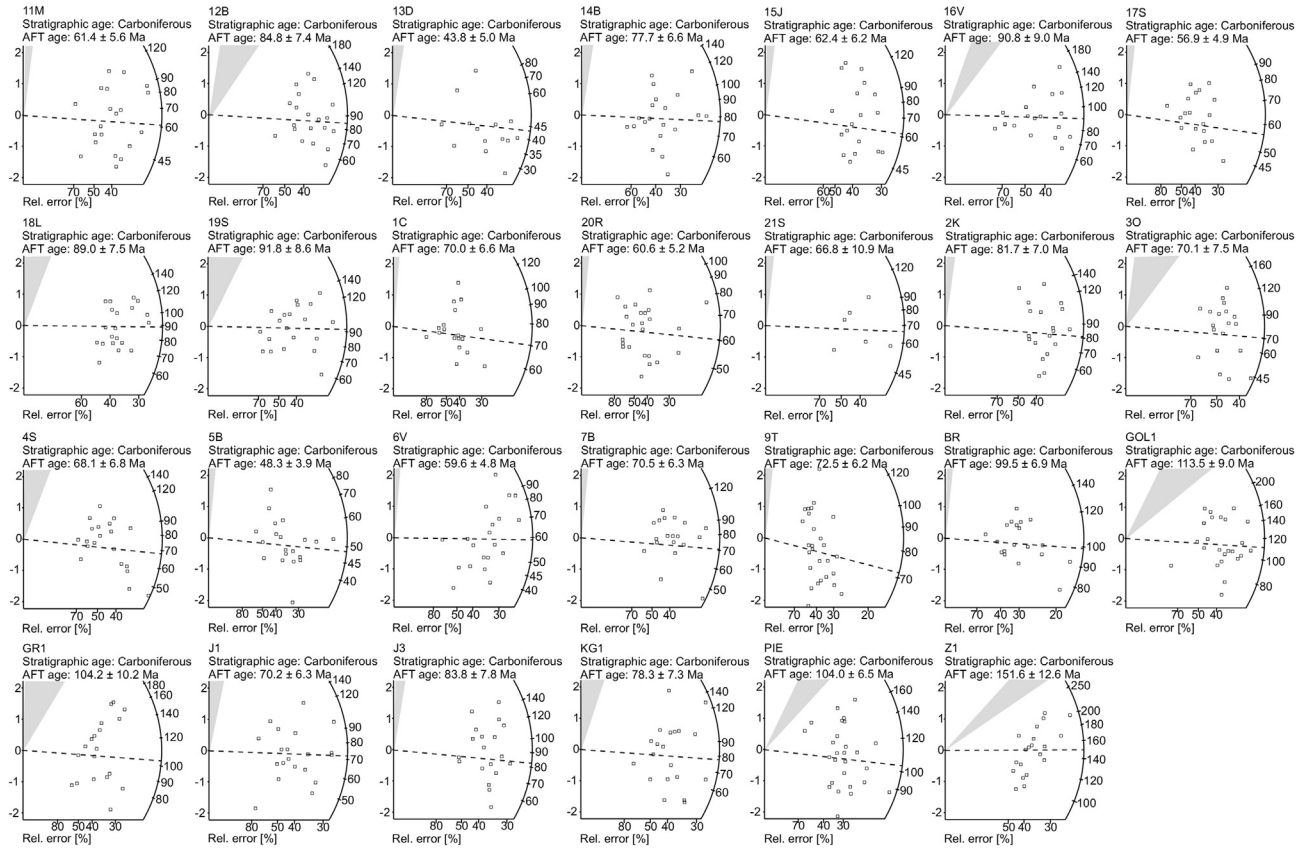


Fig. 5. Radial plots (Galbraith, 1990) of the apatite samples from the Moravo-Silesian Culm Basin, showing single grain AFT ages for each sample (in Ma).

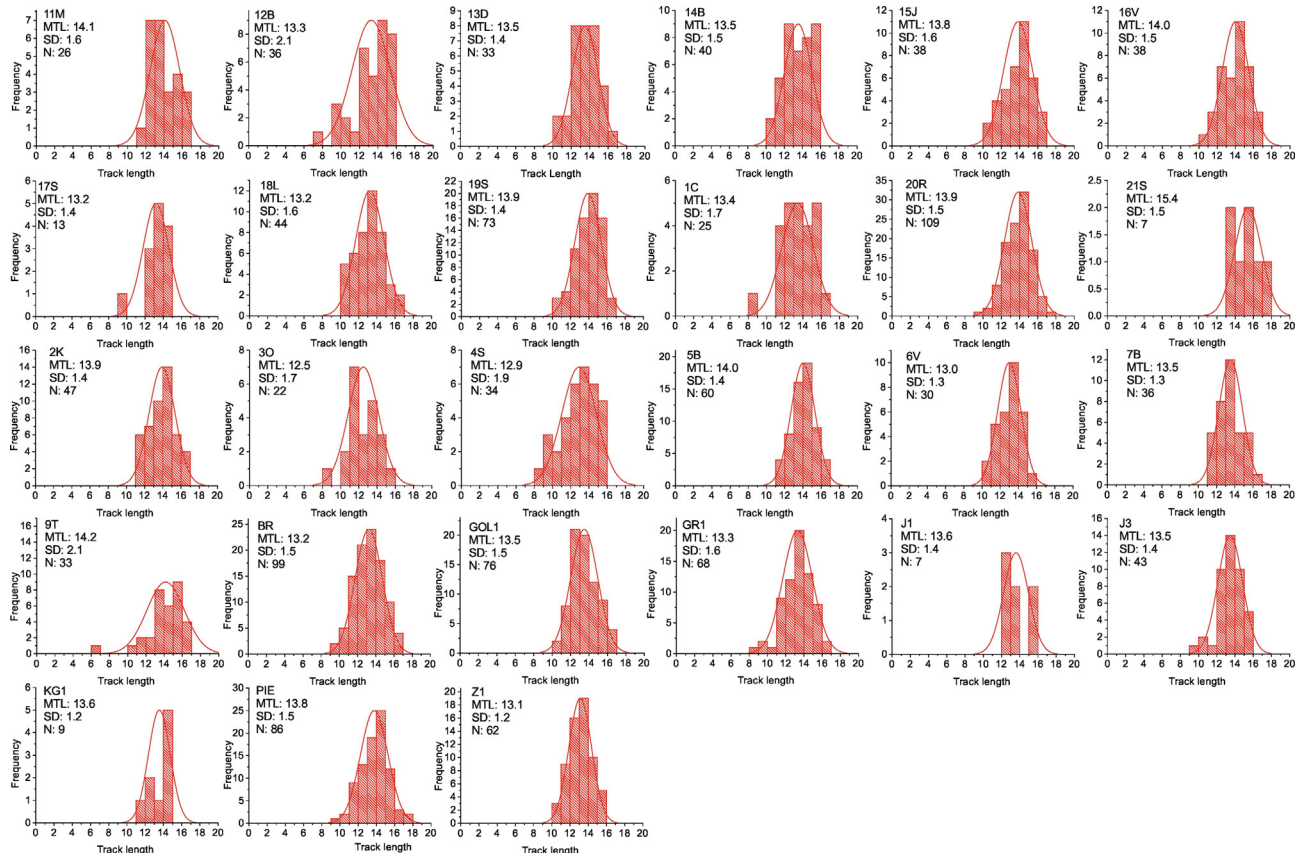


Fig. 6. Histograms of confined track lengths from the Moravo-Silesian Culm Basin.

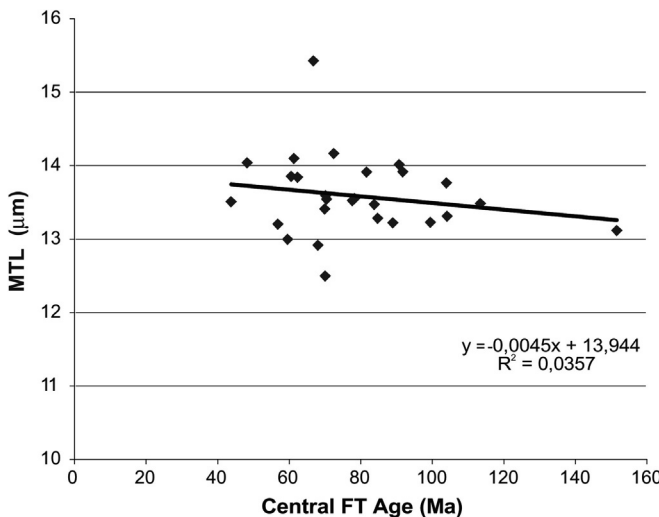


Fig. 7. Apatite central FT ages vs. mean track lengths (MTL) diagram of the samples from the Moravo-Silesian Culm Basin.

time (200–250 °C), whilst in the Late Cretaceous was lower than during the Variscan heat peak (Fig. 11) and not exceeding 100 °C (except for the 6V sample, 130 °C).

(5) As in the samples 6V and 5B none of the models, mentioned above, gave perfect results, we tested extended constraining time-temperature ranges (Fig. 12). It allows considering a much longer time of sample residence in the high temperature zone during the Mesozoic. In such a case, it does not matter if we assume a first post-Variscan cooling stage in the Permian or

later (Fig. 12B vs. A). Both models show the increase of temperature in the Early Triassic and final cooling in the Late Cretaceous/Tertiary. GOF values of these models are high (0.86–0.99). Longer residence in the higher temperature range in the Mesozoic gave better GOF values even for the samples (18L, BR) from the eastern part of the study area.

5. Discussion

The apparent ZHe ages yielded a distinct spatial pattern and increase towards the east of the study area. The range of the ZHe ages is between 303 and 233 Ma (late Carboniferous to Early Triassic), but they are significantly younger in the western part, ranging from 194 to 163 Ma (Early–Middle Jurassic). In the east of the MSCB, the late Carboniferous to Early Triassic ZHe ages may document gradual cooling after the Variscan orogeny associated with slow exhumation. A long gap between the ZHe and AFT ages suggest rather slow cooling throughout the Mesozoic. Moreover, in the western part of the Upper Silesian Coal Basin (Poland), post-Variscan heating was excluded by apatite fission track and helium thermochronology (Botor, 2014) in agreement with the results from the eastern part of the MSCB. The Early–Middle Jurassic ages in the central and western parts of study area can have twofold explanation. Firstly, they may represent cooling related to monotonous slow exhumation of the lower Carboniferous succession in association with Permian-Triassic (c. 250–245 Ma) and Middle-Jurassic (c. 170 Ma) uplift of Variscan massifs with a depositional centre located to the south of the present North Sea (Reicherter et al., 2008). This interpretation is supported by the absence of Jurassic sediments in the Sudetes, and the formation of planation surface with a low denudation rate and deep weathering in the Sudetes

Table 3

Zircon helium data.

Sample	Aliq.	He		U238				Th232				Th/U ratio	Sm			Ejection correct.	Uncorr. He-age	Ft-corr. He-age	2s	Sample unweighted aver. ± 1 s.e.
		Vol.	1s	Mass	1s	Conc.	Mass	1s	Conc.	Mass	1s	Conc.								
												[ncc]	[%]	[ng]	[%]	[ppm]	(Ft)	[Ma]	[Ma]	[Ma]
12B	1	18.0	0.9	1.256	1.8	740	0.160	2.4	94.4	0.13	0.048	6.7	28	0.717	114.0	159.0	14.8	162.9	8.8	
	2	26.1	0.9	1.594	1.8	935	0.397	2.4	233.2	0.25	0.015	13.8	9	0.705	126.6	179.6	17.3			
	3	8.1	0.9	0.572	1.8	1185	0.139	2.4	286.9	0.24	0.003	32.8	5	0.735	110.3	150.0	13.2			
18L	1	11.8	0.9	0.414	1.8	148	0.141	2.4	50.5	0.34	0.012	14.8	4	0.710	214.2	301.8	28.6	287.1	9.8	
	2	23.5	0.9	0.848	1.8	255	0.431	2.4	129.8	0.51	0.024	10.6	7	0.751	201.7	268.4	22.3			
	3	31.7	0.9	1.103	1.8	277	0.365	2.4	91.6	0.33	0.052	7.9	13	0.745	216.9	291.1	24.8			
21S	1	18.1	0.9	1.181	1.8	503	0.711	2.4	302.8	0.60	0.019	12.1	8	0.705	110.0	156.0	14.9	172.3	9.6	
	2	20.2	0.9	1.107	1.8	345	0.388	2.4	120.8	0.35	0.035	10.4	11	0.730	138.1	189.3	16.9			
	3	25.4	0.9	1.537	1.8	601	0.588	2.4	230.0	0.38	0.017	14.9	7	0.724	124.2	171.6	15.6			
5B	1	104.6	0.9	5.762	1.8	769	2.251	2.4	300.5	0.39	0.111	5.6	15	0.795	136.1	171.3	12.3	173.1	2.6	
	2	8.2	0.9	0.448	1.8	76	0.169	2.4	28.8	0.38	0.015	12.6	3	0.785	137.3	174.9	13.0			
6V	1	83.4	0.9	3.795	1.8	679	1.010	2.4	180.6	0.27	0.050	7.8	9	0.734	168.8	229.9	20.3	232.6	10.2	
	2	12.2	0.9	0.591	1.8	186	0.181	2.4	56.9	0.31	0.018	12.2	6	0.724	156.7	216.5	19.7			
	3	46.8	0.9	1.789	1.8	457	0.875	2.4	223.3	0.49	0.088	7.4	23	0.760	191.1	251.4	20.3			
7B	2	63.7	0.9	3.097	1.8	424	1.491	2.4	204.2	0.48	0.043	7.9	6	0.767	150.9	196.7	15.5	236.2	55.8	
	3	72.3	0.9	2.612	1.8	408	0.577	2.4	90.2	0.22	0.014	15.7	2	0.775	213.7	275.6	21.3			
9T	1	44.0	0.9	1.615	1.8	293	0.792	2.4	143.6	0.49	0.117	6.1	21	0.810	198.5	244.9	16.5	174.7	36.2	
	2	63.0	0.9	4.665	1.8	601	1.828	2.4	235.6	0.39	0.051	7.2	7	0.818	101.5	124.1	8.2			
	3	64.1	0.9	3.934	1.8	670	1.680	2.4	286.2	0.43	0.305	5.1	52	0.782	121.3	155.1	11.6			
GR1	2	73.6	0.9	2.442	1.8	385	0.386	2.4	60.7	0.16	0.017	12.6	3	0.762	235.7	309.4	25.1	281.4	39.6	
	3	146.9	0.9	5.392	1.8	754	2.771	2.4	387.4	0.51	0.185	4.9	26	0.781	197.9	253.3	19.0			
20R	1	81.2	1.0	4.2645712515	1.8	796	1.7430046647	2.4	325	0.41	0.0862437441	5.5	16	0.787	142.1	180.7	13.4	194.1	18.8	
	2	73.0	1.0	2.9267436803	1.8	523	1.2318834361	2.4	220	0.42	0.0430275238	6.8	8	0.800	184.9	231.2	16.4			
	3	64.6	1.0	3.7188193987	1.8	882	1.5236941707	2.4	361	0.41	0.1549667781	4.3	37	0.761	129.7	170.5	13.8			
BR	1	107.9	1.0	3.1813058946	1.8	494	0.8052988288	2.4	125	0.25	0.1376323156	4.7	21	0.781	259.0	331.5	25.3	303.1	15.9	
	2	31.4	1.0	1.0630994021	1.8	298	0.1904991932	2.4	53	0.18	0.0301762674	8.2	8	0.763	230.2	301.5	24.4			
	3	27.5	1.0	0.9918930085	1.8	319	0.4224526531	2.4	136	0.43	0.06892134	5.8	22	0.742	205.0	276.4	23.9			

Amount of helium is given in nano-cubic-cm in standard temperature and pressure.

Amount of radioactive elements are given in nanograms.

Ejection correct. (Ft): correction factor for alpha-ejection (according to Farley et al., 1996 and Hourigan et al., 2005).

Uncertainties of helium and the radioactive element contents are given as 1 sigma, in relative error %.

Uncertainty of the single grain age is given as 2 sigma and it includes both the analytical uncertainty and the estimated uncertainty of the Ft.

Uncertainty of the sample average age is given as $(SD)/(n)^{1/2}$; where SD = standard deviation of the age replicates and n = number of age determinations.

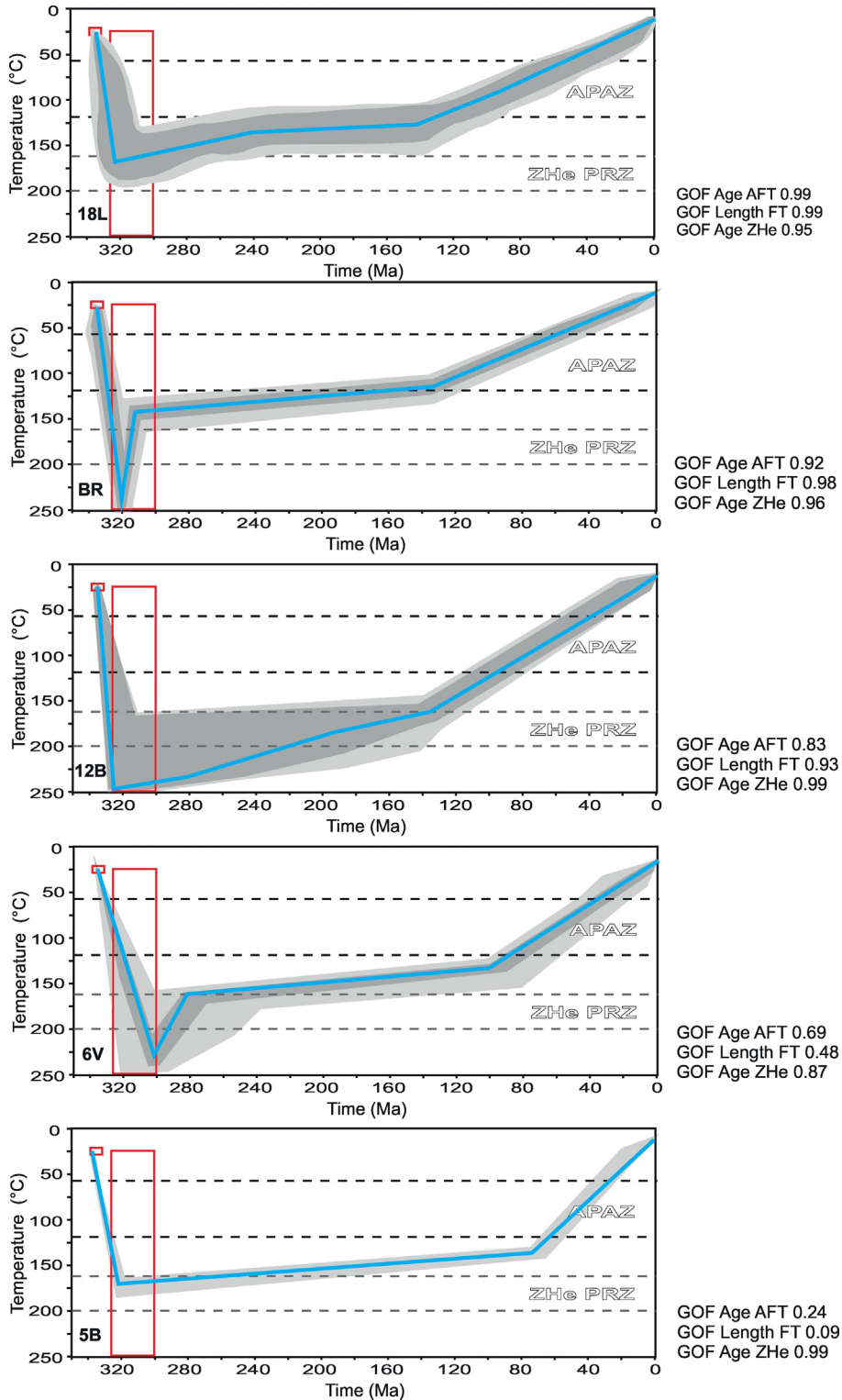


Fig. 8. Thermal modeling results for the Moravo-Silesian Culm Basin assuming heating only in the Carboniferous. See further explanation in the text.

during the Mesozoic (Migoń and Lidmar-Bergström, 2001; Ziegler and Dèzes, 2007; Danišík et al., 2010). Secondly, the ZHe ages could have been rejuvenated by a subsequent thermal event(s) due to sedimentary burial and/or a heat flow increase resulting in the helium loss and younger apparent ages (Fig. 13; compare to Danišík et al., 2012; Sobczyk et al., 2015). The ZHe ages from the western part of the MSCB implies that samples left a ~150–180 °C isotherm interval in the Early–Middle Jurassic. These ZHe ages potentially reflect some

re-heating of the lower Carboniferous rocks in the Mesozoic. Danišík et al. (2012) have documented a similar Carboniferous–Jurassic set of single grain ZHe ages from the Rychlebské Hory block, SW of the Sudetic Marginal Fault (NW of our study area), which range from ~360 to ~190 Ma. Their ZHe ages are similar to the ZHe ages in the MSCB. However, NE of the Sudetic Marginal Fault, Danišík et al. (2012) postulate significant Cretaceous burial heating based on the Late Cretaceous ZHe ages (117–72 Ma; Fig. 4).

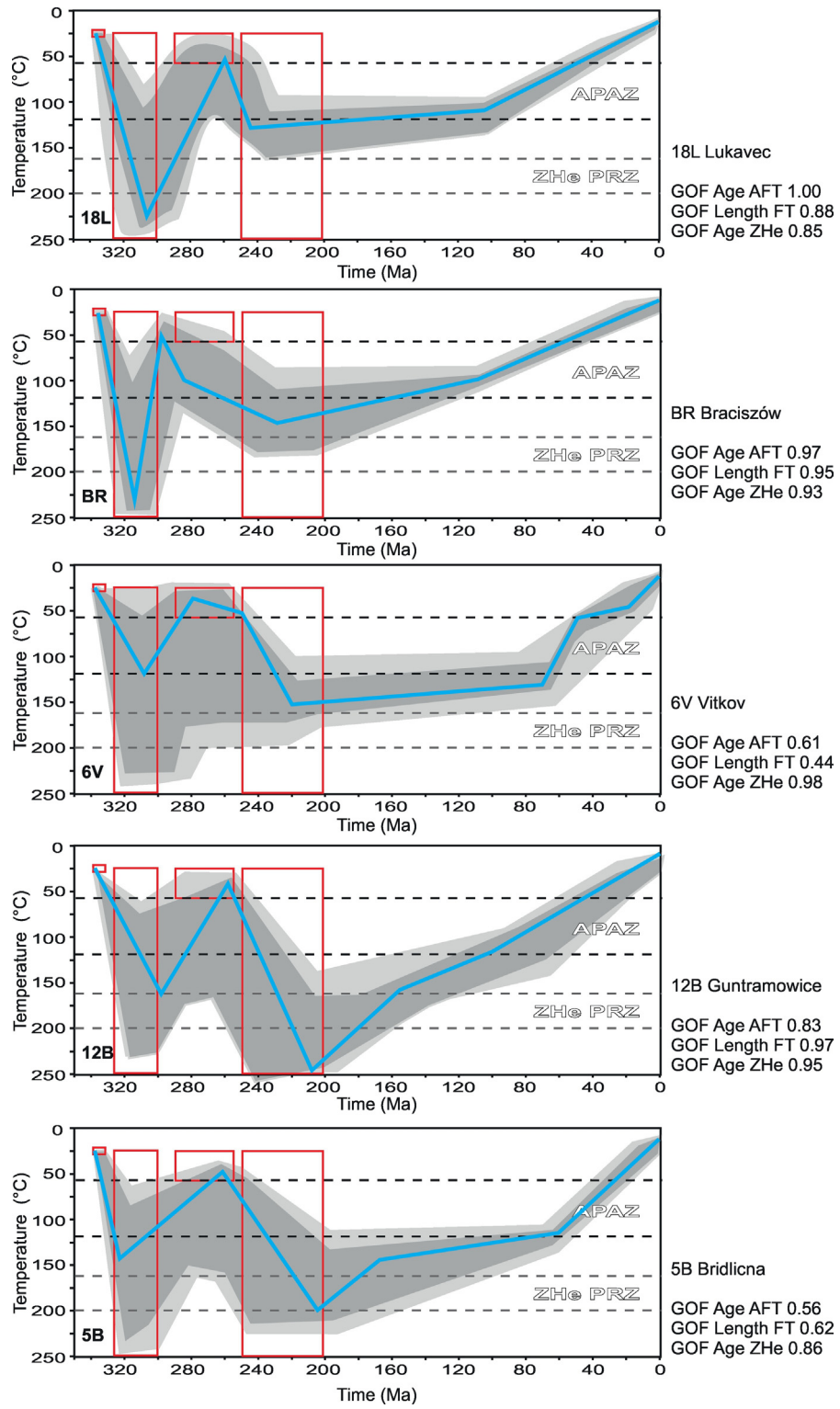


Fig. 9. Thermal modeling results for the Moravo-Silesian Culm Basin assuming Triassic re-heating. See further explanation in the text.

All measured apparent AFT ages (152 to 44 Ma) postdate Variscan burial. No particular regional pattern can be recognized according to the AFT ages. The AFT ages show similar thermal history for all samples across the basin and point to a Cretaceous to Paleogene cooling period. The AFT data document cooling after the Variscan orogeny associated with slow exhumation and finally the Late Cretaceous-Paleogene acceleration of tectonic inversion.

In the Late Triassic to Early Cretaceous, the Sudetes, including the study area, formed an emerged landmass, undergoing slow erosion,

surface lowering and weathering with the formation of thick weathering mantles (e.g., Migoń and Lidmar-Bergström, 2001; Badura et al., 2004; Danišík et al., 2012). However, in the Late Cretaceous some parts of the Sudetes were concealed beneath a significant Cretaceous sedimentary cover as postulated by Danišík et al. (2012) for the area NE of the Sudetic Marginal Fault and Sobczyk et al. (2015) for the middle part of the Sudetes. Only some erosional remnants of the Cretaceous basin still exist in the Sudetes (e.g., Skoček and Valečka, 1983; Milewicz, 1997; Uličný, 2001). The AFT ages obtained show that the

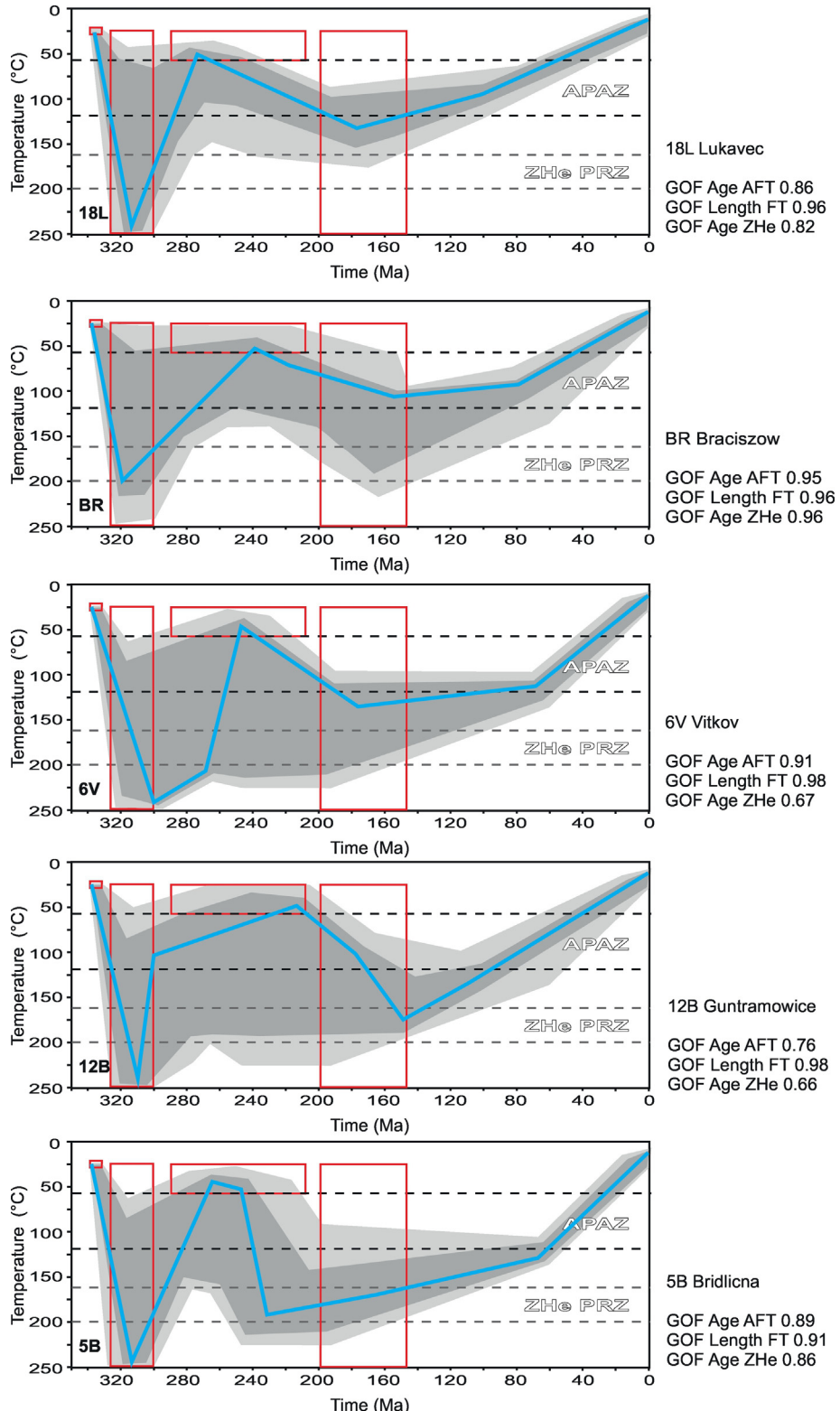


Fig. 10. Thermal modeling results for the Moravo-Silesian Culm Basin assuming Jurassic re-heating. See further explanation in the text.

presently exposed lower Carboniferous sedimentary sequence of the MSCB was at temperatures around 100 °C during the Late Cretaceous. Therefore, the rocks presently at the surface could have been at depths of ~2 to 3.5 km at that time, assuming a paleogeothermal gradient of 24 °C/km equal to the present value of 22–26 °C/km (Bruszecka, 2000; Dowgialo, 2002) and an average surface temperature of 20 °C in the Cretaceous (Thomson and Zeh, 2000). However, Dvořák (1989)

estimated in several boreholes that the Carboniferous geothermal gradient was higher than 70 °C/km in the eastern MSCB and up to 200 °C/km in the western MSCB. Although, the vertical profiles for these calculations were short, not more than a few hundred meters, these results suggest that the heat flow in the Carboniferous significantly exceeded the present-day value (see also Bábek et al., 2005). Botor et al. (2017) has shown that a geothermal gradient was at least 50 °C/km based on

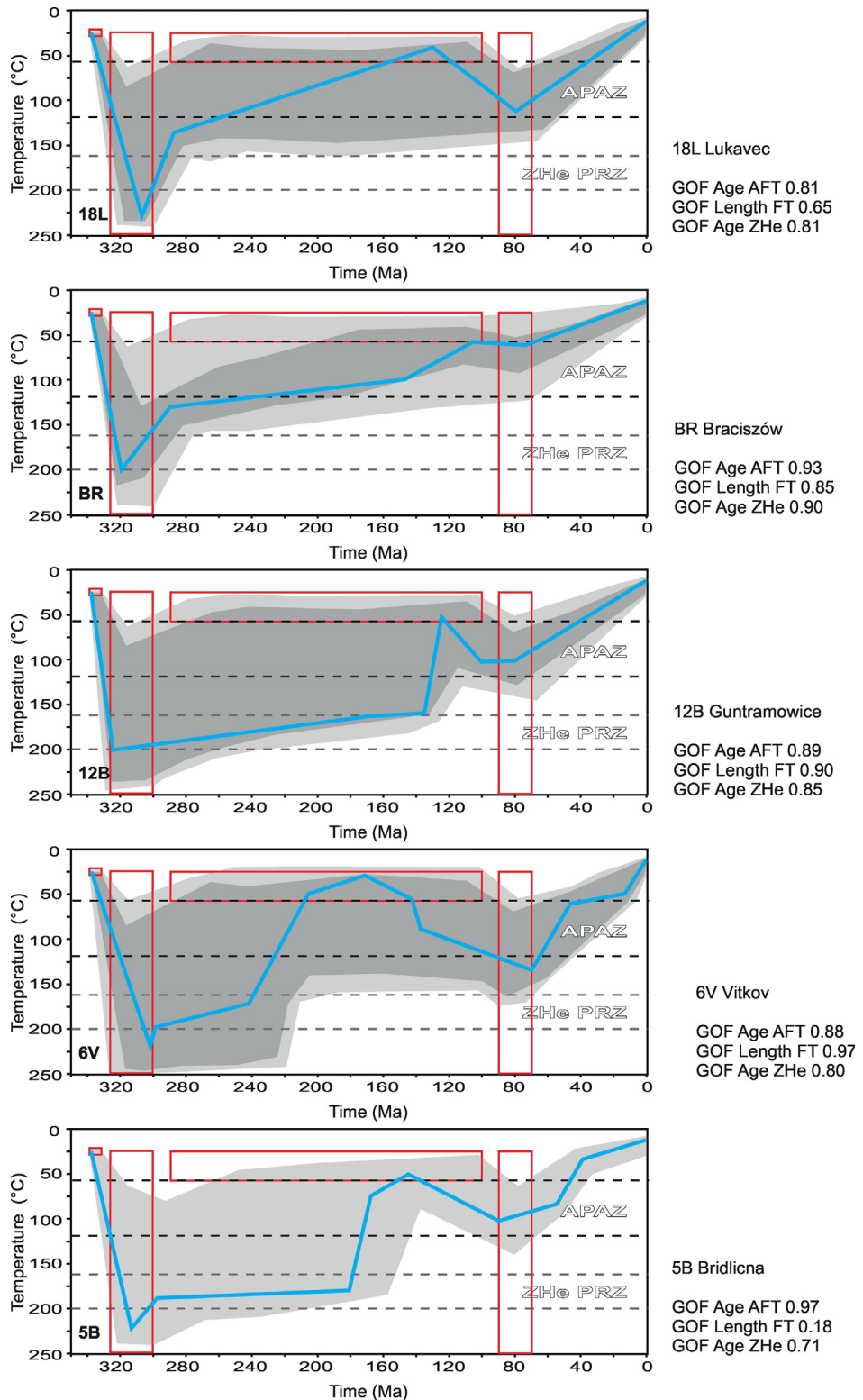


Fig. 11. Thermal modeling results for the Moravo-Silesian Culm Basin assuming Cretaceous re-heating. See further explanation in the text.

the fluid inclusion data in the western part of the MSCB. We have also calculated a geothermal gradient for the lower Carboniferous strata based on the VR data from the Fosowskie IG-2 borehole (see Fig. 1 for location) given by Nowak (2003), who measured VR from 2.3 to 4.6% in a depth range of 723 m to 1618 m. In this case, vitrinite reflectance has been used as an input parameter for the estimation of maximum paleotemperature after Barker and Pawlewicz (1994). In the present

study, the formula: $T_B = (\ln VR + 1.68)/0.0124$ for the burial heating model and $T_H = (\ln VR + 1.19)/0.00782$ for the hydrothermal heating model after Barker and Pawlewicz (1994) is used. The formula is calibrated up to 7% VR (Barker and Pawlewicz, 1994). The calculated geothermal gradient was from 60 °C/km (using T_B) to 100 °C/km (using T_H). The above-mentioned studies show that the Carboniferous geothermal gradient was presumably at least twice as high as present-day

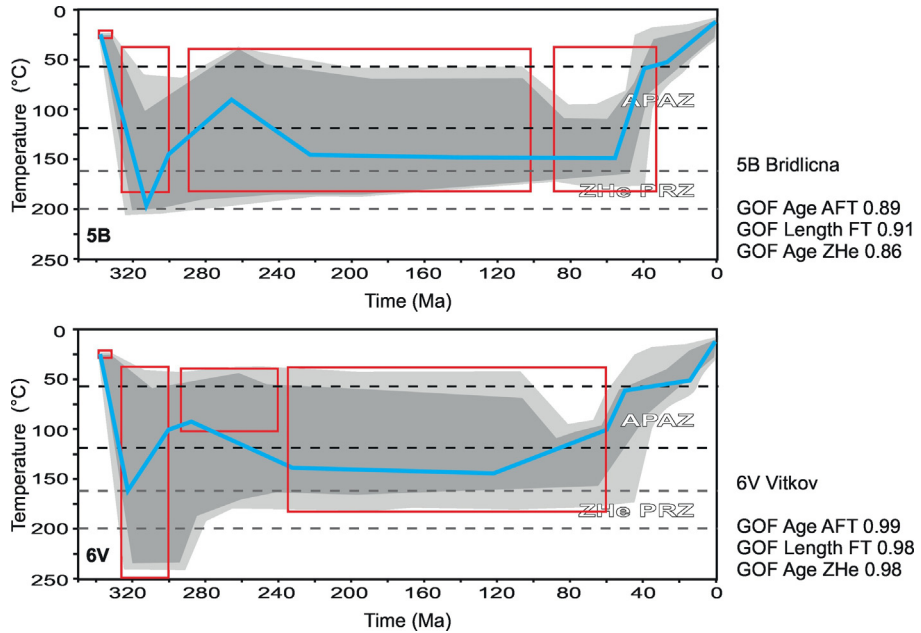


Fig. 12. Thermal modeling results for the Moravo-Silesian Culm Basin assuming Triassic re-heating followed by residence in the range of 120–180 °C (apatite annealing zone) until the Late Cretaceous. See further explanation in the text.

values. Considering the above data and assuming a gradient of 50 °C/km, the rocks presently at the surface could have been at depths of ~1 to 1.7 km at the time of maximum burial. As no significant differences exist between the AFT ages from different localities, the presently exposed rocks were almost at the same temperature during the Late Cretaceous. Since there are no younger sediments in the immediate vicinity of the MSCB (Fig. 1) increased heat flow seems to be a major contributing factor of heating instead of burial.

Generally, the best fit of thermal modeling results (Figs. 8–12, Table 4) and thermochronological data was achieved by applying the Variscan

heat peak, Permian cooling and Mid-Late Triassic re-heating. However, the temperature need to be in a relatively high range (~120–150 °C) until the Cretaceous to get better GOF values in all the analysed models (Fig. 12). Finally, a common feature of all models is relatively fast cooling in the Late Cretaceous-Paleogene. Therefore, Mesozoic re-heating of the MSCB seems to be the most plausible explanation of the post-Variscan thermal history. Also Vamvaka et al. (2014), based on the AFT study in the southern part of the Bohemian Massif, concluded that a full explanation of the AFT age record must accept higher crustal heat flow in the Mesozoic (Mid- to Late Jurassic). This increase in heat

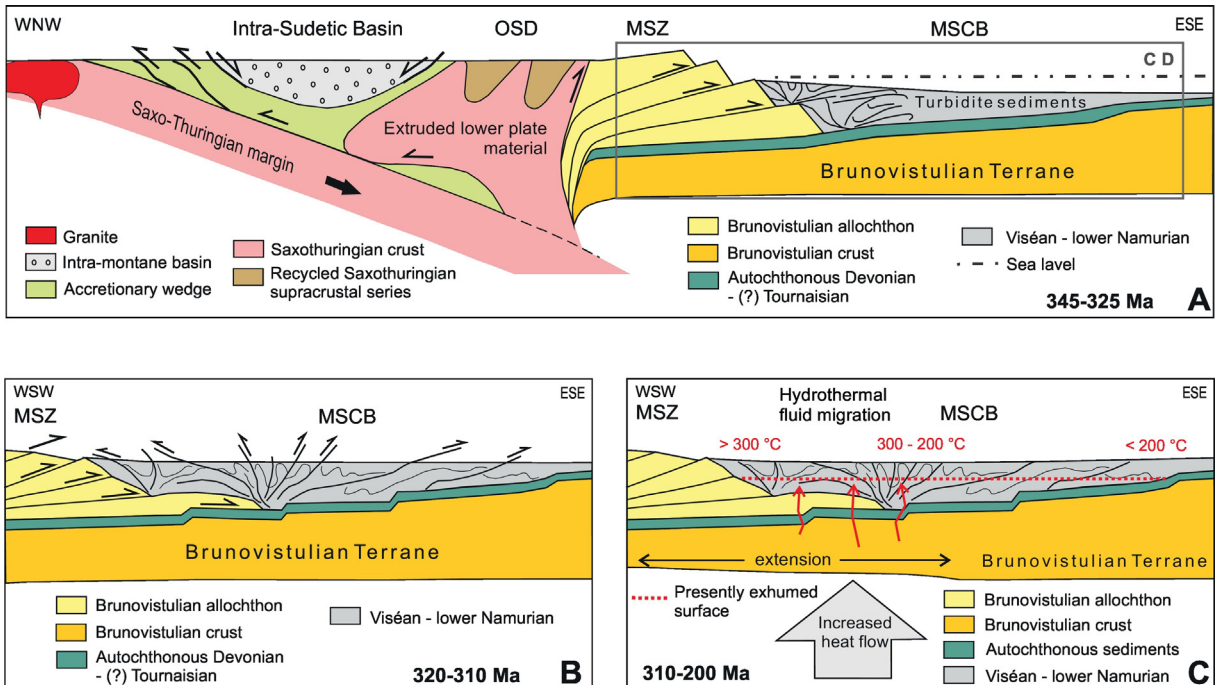


Fig. 13. Simplified conceptual model of the thermal evolution of the Moravo-Silesian Culm Basin. A – Schematic model showing tectonic setting of the Moravo-Silesian Culm Basin (partly after Mazur et al., 2012); B – Inversion of the Moravo-Silesian Culm Basin (partly after Grygar and Vavro, 1995); C – Reheating of basement rocks due to an early Mesozoic extensional event. Maximum paleotemperature values are based on Fig. 3. See further explanation in the text. MSCB – Moravo-Silesian Culm Basin; MSZ – Moravo-Silesian Zone; OSD – Orlica-Śnieżnik Dome.

flow may have been caused by extension and lithospheric thinning resulting in a higher geothermal gradient (Vamvaka et al., 2014). The thin Mesozoic overburden in the MSZ does not support any re-heating due to burial (Malkovský, 1987; Adámek, 2005; McCann et al., 2006). Moreover, in the Carboniferous basement of the Fore-Sudetic Monocline, a late Permian to Early Jurassic thermal event has been recently established from the illite K-Ar and ZHe ages (Kowalska et al., 2015).

Organic maturity and clay minerals data suggest maximum palaeotemperatures of ~200–350 °C in the MSCB (Fig. 3). Particularly in the western part of the study area, coalification thermal maturity pattern varies considerably, and its origin has not been yet fully understood (Bábek et al., 2006). The elevated vitrinite reflectance values can be ascribed to the localized influence of hot fluids that have migrated along permeable faults, thrust planes and detachment zones, and could be heat carriers increasing the coalification (e.g., Lüneneschloss et al., 1997). The thermal maturity pattern in the Nízký Jeseník section of the MSCB has been recently explained by (1) Variscan (mid-late Carboniferous) burial diagenesis, and (2) a post-Variscan, probably mid-Mesozoic, thermal pulse, related to advective heat transport and circulation of fluids that overprinted the Variscan maturity, particularly in the central and western parts of the MSCB (Botor et al., 2017). The Raman spectroscopy-based maximum paleotemperature (T_{RSCM}) shows increasing thermal maturity of organic matter from the east to west (Botor et al., 2017). Moreover, the T_{RSCM} is compatible with the VR-derived paleotemperature (using equations given by Barker and Pawlewicz, 1994) based on the burial model in the east and the hydrothermal model in the central and western parts of the MSCB (Botor et al., 2017). It is also worthy noticing that the study area is intersected by several major faults that could be active heat conduits in an extensional regime of the post-Variscan period (e.g., Špacek et al., 2015).

The results presented in this paper are consisted with structural evidence available from the MSCB and the adjacent units and can be incorporated in a tectonic scenario build upon previously published data (Fig. 13). These results also allow addressing some aspects related to the structural evolution of the MSCB that so far remained unconstrained. The overall tectonics of the MSFTB and the adjacent MSCB is the result of the collisional interaction of the Brunovitulian Neoproterozoic-age basement microplate with the Saxothuringian Terrane incorporated within the Variscan Belt (Fig. 13A; e.g., Chopin et al., 2012; Mazur et al., 2012; Janoušek et al., 2014) and it is likely to contain a more significant NNE–SSW directed strike-slip component than has been assumed to date (Rajlich, 1990; Schulmann et al., 1991; Schulmann and Gayer, 2000), but whose effects are, however, thus far poorly recognized and unconstrained. The ongoing convergence led to the collision of both terranes and emplacement of crystalline nappes that were thrust north-eastwards over the Brunovitulian foreland during the Viséan. They created a tectonic load resulting in flexural subsidence of the foreland and extensive Culm succession deposition within the MSCB (Fig. 13A).

Late phases of convergence led to shortening and deformation of the MSCB that presently shows a thin-skinned structural style (Fig. 13B). There is no sharp frontal thrust separating the MSFTB from the foreland basin and deformation gradually fades out eastwards. Folding and thrusting within the MSFTB contributed to burial heating of the Culm facies clastics by a tectonic increase of the overburden. The Variscan convergence waned at the end of Carboniferous and it was directly replaced by rift-related lithospheric thinning (e.g., Wilson et al., 2004; Turniak et al., 2014). A general extensional regime prevailed in Central Europe until the Late Cretaceous with several pulses of renewed tectonic extension recorded in the sediments of the adjacent Permo-Mesozoic Polish Basin (see Krzywiec, 2009 for overview). The scarcity of Mesozoic, pre-Late Cretaceous sediments in the Sudetes prevents direct evidence when and to what extent these extensional episodes affected the elevated Variscan basement of the Bohemian Massif. However, Mesozoic remagnetisation of the Sudetic basement rocks provides indirect evidence for tectonic extension, reheating and fluid circulation (Kądziałko-Hofmokl et al., 2003, 2013). The current study supplements

Table 4
Results of HeTy thermal modeling.

Sample	Heating Variscan in Carboniferous	Re-heating post-Variscan		
		In Triassic	In Jurassic	In Cretaceous
18L	3	2	2	0
BR	3	3	3	2
6V	0	3*	2	0
12B	2	2	1	1
5B	0	3*	2	0

Modeling quality based on all GOF values for single model.

3: excellent match, 2: fair match, 1: bad match, 0: no match.

3* if sample stay till Cretaceous.

additional arguments in favour of Mesozoic thermal events the most important of which would be of the Mid- to Late Triassic age (Fig. 13C). This seems to be a plausible scenario since the present-day Bohemian Massif was at that time part of European hinterland adjoining an active margin of the Tethys Ocean in the south (e.g., Golonka et al., 2003).

6. Conclusions

The apparentapatite fission-track ages obtained range from 152 Ma to 44 Ma, but most of them are Late Cretaceous. The mean track length is ranging from 12.5 to 15.4 μm in the studied samples. The unimodal track length distributions, the relatively short mean track length, and the low standard deviation values (1.2 to 2.1 μm) imply a thermal history that was determined by Variscan and post-Variscan heating events followed by a prolonged residence in theapatite partial annealing zone in the Mesozoic concluded by cooling in the Paleogene. The AFT data indicate relatively faster cooling during the Late Cretaceous and Paleogene.

The apparent zircon (U-Th)/He ages are scattered with the range of 303 to 233 Ma (late Carboniferous to Early Triassic); they are significantly younger in the western part, ranging from 194 to 163 Ma (Early–Middle Jurassic). All the samples experienced a substantial post-depositional thermal reset; both the AFT and ZHe ages are considerably younger than the depositional ages. The ZHe data and thermal modeling results show reheating in the Permian and Triassic that was probably triggered by extensional tectonics. The extensional regime might have caused high heat flow that overprinted the former burial-related maturation of organic matter and contributed to resetting of the AFT and ZHe thermochronometers. A relatively poor-match was found by means of thermal modeling for the Mesozoic reheating scenarios in the east of the MSCB. These results suggest that a Permian-Triassic thermal pulse was limited to the western and central parts of the basin. The MSCB was heated firstly by Variscan burial diagenesis, and later by post-Variscan thermal pulses related to crustal extension and advective heat transport that overprinted the Variscan basement in the central and western parts of the MSCB.

Acknowledgements

We thank Mateusz Rechowicz and Anna Zagórska for mineral separation of greywacke samples, Reinhard Wolff for reading of the early version of the manuscript, and two anonymous reviewers for their valuable input, which improved the quality of the paper. AFT measurements were financed by AGH statutory grant no. 11.11.140.562, whilst ZHe dating by ATLAB REGPOT-2011-1 EU FP7.

Appendix A. Supplementary data

Supplementary data associated with this article can be found in the online version, at <http://dx.doi.org/10.1016/j.tecto.2017.06.035>. These data include the Google map of the most important areas described in this article.

References

- Adámek, J., 2005. The Jurassic floor of the Bohemian Massif in Moravia: geology and paleogeography. *Bull. Geosci.* 80 (4), 291–305.
- Aramowicz, A., Añczkiewicz, A.A., Mazur, S., 2006. Fission track dating of apatites from the Góry Sowie Massif, Polish Sudetes, NE Bohemian Massif: implications of post-Variscan denudation and uplift. *Neues Jb. Mineral. Abh.* 182 (3), 221–229.
- Bábek, O., Franců, E., 2004. Regional trends in thermal maturity of Paleozoic rocks of the Moravo-Silesian Basin: a combined study of Conodont Alteration Index (CAI), vitrinite reflectance and rock eval pyrolysis. *GeoLines* 17, 6–17.
- Bábek, O., Mikuláš, R., Zapletal, J., Lehotský, T., 2004. Combined tectonic-sediment supply driven cycles in a Lower Carboniferous deep-marine foreland basin, Moravice Formation, Czech Republic. *Int. J. Earth Sci.* 93, 241–261.
- Bábek, O., Tomek, C., Neubauer, F., Franců, E., Kalvoda, J., Franců, E., 2005. Thermal overprint in Paleozoic sediments of the Moravo-Silesian Zone, Bohemian massif: a record of Late Variscan orogen-parallel extension. *Andean Geol.* 19, 17.
- Bábek, O., Tomek, C., Melichar, R., Kalvoda, J., Otava, J., 2006. Structure of unmetamorphosed Variscan tectonic units of the southern Moravo-Silesian Massif: a review. *Neues Jahrb. Geol. Paläontol. Abh.* 239, 37–75.
- Bábek, O., Franců, E., Kalvoda, J., Neubauer, F., 2008. A digital image analysis approach to measurement of the conodont colour alteration index (CAI): a case study from the Moravo-Silesian Zone, Czech Republic. *Neues Jb. Geol. Paläontol. Abh.* 249, 185–201.
- Badura, J., Przybylski, B., Zuchiewicz, W., 2004. Cainozoic evolution of Lower Silesia, SW Poland: a new interpretation in the light of sub-Cainozoic and sub-Quaternary topography. *Acta Geodyn. Geomater.* 1 (3), 135.
- Badura, J., Pécskay, Z., Koszowska, E., Wolska, A., Zuchiewicz, W., Przybylski, B., 2005. New age and petrological constraints on Lower Silesian basaltoids. SW Poland. *Acta Geodyn. Geomater.* 2–3/139, 7–15.
- Barker, C., Pawlewicz, M.J., 1994. Calculation of vitrinite reflectance from thermal histories: a comparison of methods. In: Mukhopadhyay, P.K., Dow, W.G. (Eds.), *Vitrinite Reflectance as a Maturity Parameter: Applications and Limitations*. American Chemical Society Symposium Series 570, pp. 216–229.
- Bieracka, J., Józefiak, M., 2009. The Eastern Sudetic Island in the Early-to-Middle Turonian: evidence from heavy minerals in the Jerzmanice sandstones, SW Poland. *Acta Geol. Pol.* 59, 545–565.
- Birkenmajer, K., Jelenska, M., Kadzialko-Hofmokl, M., Kruczyk, J., 1977. Age of deep-seated fractures zones in Lower Silesia (Poland), based on K-Ar and paleomagnetic dating of Tertiary basalts. *Roczn. Pol. Towarz. Geol.* 47, 545–552.
- Birkenmajer, K., Pécskay, Z., Grabowski, J., Lorenc, M.W., Zagozdzon, P.P., 2002a. Radiometric dating of the Tertiary volcanics in Lower Silesia, Poland. Part II. K-Ar and palaeomagnetic data from Neogene basanites near Ladek Zdrój, Sudetes Mts. *Ann. Soc. Geol. Pol.* 72, 119–129.
- Birkenmajer, K., Pécskay, Z., Grabowski, J., Lorenc, M.W., Zagozdzon, P.P., 2002b. Radiometric dating of the Tertiary volcanics in Lower Silesia, Poland. Part III. K-Ar and palaeomagnetic data from early Miocene basaltic rocks near Jawor, Fore-Sudetic Block. *Ann. Soc. Geol. Pol.* 72, 241–253.
- Birkenmajer, K., Pécskay, Z., Grabowski, J., Lorenc, M.W., Zagozdzon, P.P., 2004. Radiometric dating of the Tertiary volcanics in Lower Silesia, Poland. Part IV. Further K-Ar and paleomagnetic data from late Oligocene to early Miocene basaltic rocks of the Fore-Sudetic block. *Ann. Soc. Geol. Pol.* 74, 1–19.
- Bischoff, R., Semmel, A., Wagner, G.A., 1993. Fission-track analysis and geomorphology in the surroundings of the drill site of the German Continental Deep Drilling Project (KTB)/Northeast Bavaria. *Z. Geomorphol. Suppl.* 92, 127–143.
- Botor, D., 2014. Timing of coalification of the Upper Carboniferous sediments in the Upper Silesia Coal Basin (SW Poland) on the basis of byapatite fission track and helium dating. *Gospodarka Surowcami Mineralnymi – Miner. Resour. Manag.* 30 (1), 85–104.
- Botor, D., Añczkiewicz, A.A., 2015. Thermal history of the Sabero Coalfield (Southern Cantabrian Zone, NW Spain) as revealed by apatite fission-track analyses from tonstein horizons: implications for timing of coalification. *Int. J. Earth Sci.* 104, 1779–1793.
- Botor, D., Tobola, T., Jelonek, I., 2017. Thermal history of Lower Carboniferous MSCB in the Nízký Jeseník Mts. (Moravo-Silesian Zone, NE Bohemian Massif, Czech Republic-Poland): combined data from Raman spectroscopy of carbonaceous material, vitrinite reflectance and fluid inclusions. *Annales Societatis Geologorum Poloniae* 87. <http://dx.doi.org/10.14241/asgp.2017.002>.
- Bruszecka, B., 2000. The geothermal conditions in Lower Silesia (SW Poland). *Prz. Geol.* 48, 639–643.
- Cháb, J., 1990. The problem of the Andelská hora thrust in the light of new deep boreholes (Hrubý Jeseník Mts.). *Časopis pro mineralogii a geologii* 35, 389–401.
- Cháb, J., Fediukova, E., Fisera, M., Novotny, P., Opletal, M., 1990. Variscan orogeny in the Silesicum (in Czech). *Sborník geologických věd, Ložisková geologie-mineralogie* 29, 9–39.
- Chadima, M., Hrouda, F., Melichar, R., 2006. Magnetic fabric study of the SE Rhenohercynian Zone (Bohemian Massif): implications for dynamics of the Paleozoic accretionary wedge. *Tectonophysics* 418, 93–109.
- Chopin, F., Schulmann, K., Skrzypek, E., Lehmann, J., Dujardin, R., Martelat, J.E., Lexa, O., Corsini, M., Edel, J.B., Štípká, P., Pitra, P., 2012. Crustal influx, indentation, ductile thinning and gravity redistribution in a continental wedge: building a Moldanubian mantled gneiss dome with underthrust Saxothuringian material (European Variscan belt). *Tectonics* 31:TC1013. <http://dx.doi.org/10.1029/2011TC002951>.
- Čížek, P., Tomek, C., 1991. Large-scale thin-skinned tectonics in the Eastern boundary of the Bohemian Massif. *Tectonics* 10 (2), 273–286.
- Coyle, D.A., Wagner, G.A., Hejl, E., Brown, R., Van den Haute, P., 1997. The Cretaceous and younger thermal history of the KTB site (Germany): apatite fission-track data from the Vorbohrung. *Geol. Rundsch.* 86, 203–209.
- Dallmeyer, R.D., Neubauer, F., Hock, V., 1992. Chronology of late Paleozoic tectonothermal activity in the southeastern Bohemian Massif, Austria (Moldanubian and Moravo-Silesian zones): 40Ar/39Ar mineral age controls. *Tectonophysics* 210, 135–153.
- Danišák, M., Migoň, P., Kuhlemann, J., Evans, N.J., Dunkl, I., Frisch, W., 2010. Thermochronological constraints on the long-term erosional history of the Karkonosze Mts., Central Europe. *Geomorphology* 117, 78–93.
- Danišák, M., Štěpančíková, P., Evans, N.J., 2012. Constraining long-term denudation and faulting history in intraplate regions by multi-system thermochronology – an example of the Sudetic Marginal Fault (Bohemian Massif, Central Europe). *Tectonics* 31 (2):1–19. <http://dx.doi.org/10.1029/2011TC003012>.
- Demek, J., 1975. Planation surfaces and their significance for the morphostructural analysis of the Czech Socialist Republic. *Stud. Geogr.* 54, 133–164.
- Dézes, P., Schmid, S.M., Ziegler, P.A., 2004. Evolution of the European Cenozoic Rift System: interaction of the Alpine and Pyrenean orogens with their foreland lithosphere. *Tectonophysics* 389 (1), 1–33.
- Dolníček, Z., René, M., Hermannová, S., Prochaska, W., 2014. Origin of the Okrouhlá Radouň episyenite-hosted uranium deposit, Bohemian Massif, Czech Republic: fluid inclusion and stable isotope constraints. *Mineral. Deposita* 49, 409–425.
- Donelick, R.A., Ketcham, R.A., Carlson, W.D., 1999. Variability of apatite fission track annealing kinetics: II. Crystallographic orientation effects. *Am. Mineral.* 84, 1224–1234.
- Donelick, R.A., O'Sullivan, P.B., Ketcham, R.A., 2005. Apatite fission track analysis. *Rev. Mineral. Geochem.* 58, 49–94.
- Dowgiatko, J., 2002. The Sudetic geothermal region of Poland. *Geothermics* 31 (3), 343–359.
- Dudek, A., 1980. The crystalline basement block of the outer Carpathians in Moravia: Bruno-Vistulicum. *Rozpravy České akademie věd* 90, 1–85.
- Dumitru, T., 1993. A new computer-automated microscope stage system for fission track analysis. *Nucl. Tracks Radiat. Meas.* 21, 575–580.
- Dunkl, I., 2002. TrackKey: a Windows program for calculation and graphical presentation of fission track data. *Comput. Geosci.* 28, 3–12.
- Dvořák, J., 1973. Synsedimentary tectonics of the Paleozoic of the Drahany Upland (Sudeticum, Moravia, Czechoslovakia). *Tectonophysics* 17, 359–391.
- Dvořák, J., 1989. Anchimetamorphism in the Variscan tectogene in Central Europe: its relationship to tectogenesis. *Vstník Ústředního Ústavu Geologického* 64, 17–30 (in Czech with English abstract).
- Dvořák, J., 1994. Variscan flysch development in the Nízký Jeseník Mts. in Moravia and Silesia (in Czech with English summary). *Czech Geological Survey Prague*. (1–117 pp).
- Dvořák, J., Paproth, E., 1969. Über die Position und die Tektonik des Rhenohercyniums und des Sudetikums des mitteleuropäischen Varisziden (in German). *Neues Jahrbuch für Geologie und Paläontologie, Monatshefte*, pp. 65–88.
- Dvořák, J., Wolf, M., 1979. Thermal metamorphism in the Moravian Paleozoic (Sudeticum, CSSR). *Neues Jb. Geol. Paläontol. Monat.* 1979–10, 596–607.
- Dyjor, S., 1986. Evolution of sedimentation and palaeogeography of near-frontier areas of the Silesian part of Paratethys and of the Tertiary Polish-German basin. *Zeszyty Naukowe AGH* 1077. *Geologia* 12, 7–23.
- Eliáš, M., 1981. Facies and paleogeography of the Jurassic of the Bohemian Massif. *Sborník geologických věd, Geologie* 35, 75–144.
- Farley, K.A., 2002. (U-Th)/He dating: techniques, calibrations, and applications. *Rev. Mineral. Geochem.* 47 (1), 819–844.
- Farley, K.A., Wolf, R.A., Silver, L.T., 1996. The effects of long alpha-stopping distances on (U-Th)/He ages. *Geochim. Cosmochim. Acta* 60 (21), 4223–4229.
- Feist-Burkhardt, S., Götz, A.E., Szulc, J., Borkhataria, R., Geluk, M., Haas, J., Hornung, J., Jordan, P., Kempf, O., Michalik, J., Nawrocki, J., Reinhardt, L., Ricken, W., Röhling, H.G., Rüffer, T., Török, Á., Zühlke, R., 2008. *Triassic: The Geology of Central Europe. Vol. 2. The Geological Society, London*, pp. 749–822.
- Filip, J., Suchý, V., 2004. Thermal and tectonic history of the Barrandian Lower Paleozoic, Czech Republic: is there a fission-track evidence for Carboniferous-Permian overburden and pre-Westphalian alpinotype thrusting? *Bull. Geosci.* 79, 107–112.
- Filip, J., Ulrych, J., Adamovič, J., Balogh, K., 2007. Apatite fission track implication for timing of hydrothermal fluid flow in Tertiary volcanics of the Bohemian Massif. *J. Geosci.* 52, 211–220.
- Franců, E., Franců, J., Kalvoda, J., 1999. Illite crystallinity and vitrinite reflectance in Paleozoic siliciclastics in the SE Bohemian Massif as evidence of thermal history. *Geol. Carpath.* 50, 365–372.
- Franců, E., Franců, J., Kalvoda, J., Polcheau, H.S., Otava, J., 2002. Burial and uplift history of the Palaeozoic Flysch in the Variscan foreland basin (SE Bohemian Massif, Czech Republic). *EGS Stephen Mueller Special Publication Series* 1, pp. 259–278.
- Franke, W., 1995. Rhenohercynian foldbelt; Autochthon and nonmetamorphic nappe units: stratigraphy. In: Dallmeyer, R.D., Franke, W., Weber, K. (Eds.), *Pre-Permian geology of Central and Eastern Europe*. Springer, Berlin, pp. 33–49.
- Franke, W., Żelaźniewicz, A., 2000. The eastern termination of the Variscides: terrane correlation and kinematic evolution. In: Franke, W., Haak, V., Oncken, O., Tanner, D. (Eds.), *Orogenic Processes: Quantification and Modelling in the Variscan Belt*. *Geological Society of London Special Publications* 179, pp. 63–86.
- Fritz, H., Neubauer, F., 1995. Moravo-Silesian Zone; autochthon; structure. In: Dallmeyer, R.D., Franke, W., Weber, K. (Eds.), *Pre-Permian geology of Central and Eastern Europe*. Springer, Berlin, pp. 490–494.
- Galbraith, R.F., 1981. On statistical models for fission track counts. *Math. Geol.* 13 (6), 471–478.
- Galbraith, R.F., 1990. The radial plot: graphical assessment of spread in ages. *Nucl. Tracks Radiat. Measur.* 17, 207–214.
- Galbraith, R.F., Laslett, G.M., 1993. Statistical models for mixed fission track ages. *Nucl. Tracks Radiat. Measur.* 21 (4), 459–470.
- Glasmacher, U.A., Mann, U., Wagner, G.A., 2002. Thermotectonic evolution of the Barrandian, Czech Republic, as revealed by apatite fission-track analysis. *Tectonophysics* 359, 381–402.

- Gleadow, A.J.W., Duddy, I.R., Green, P.F., Lovering, J.F., 1986. Confined fission track lengths in apatite: a diagnostic tool for thermal history analysis. *Contrib. Mineral. Petrol.* 94 (4), 405–415.
- Golonka, J., Krobicki, M., Oszczypko, N., Ślączka, A., Słomka, T., 2003. Geodynamic evolution and palaeogeography of the Polish Carpathians and adjacent areas during Neo-Cimmerian and preceding events (latest Triassic-earliest Cretaceous). In: McCann, T., Saintot, A. (Eds.), *Tracing Tectonic Deformation Using the Sedimentary Record*. Geological Society, London, Special Publications 208(1), pp. 137–158.
- Green, P.F., 1981. 'Track-in-track' length measurements in annealedapatites. *Nucl. Tracks* 5, 12–18.
- Green, P.F., Duddy, I.R., Gleadow, A.J.W., Tingate, P.R., Laslett, G.M., 1986. Thermal annealing of fission tracks in apatite: 1. A qualitative description. *Chem. Geol.: Isot. Geosci.* Sect. 59, 237–253.
- Grygar, R., Vavro, M., 1995. Evolution of Lusatian Orogen (North-eastern periphery of the Bohemian Massif): kinematics of Variscan deformation. *J. Czech Geol. Soc.* 40, 65–90.
- Hartley, A.J., Otava, J., 2001. Sediment provenance and dispersal in a deep marine foreland basin: the Lower Carboniferous Culm Basin, Czech Republic. *J. Geol. Soc. Lond.* 158, 137–150.
- Hejl, E., Coyle, D., Lal, N., Van den Haute, P., Wagner, G.A., 1997. Fission-track dating of the western border of the Bohemian massif: thermochronology and tectonic implications. *Geol. Rundsch.* 86, 210–219.
- Hejl, E., Sekyra, G., Friedl, G., 2003. Fission-track dating of the south-eastern Bohemian Massif (Waldbüttel, Austria): thermochronology and long-term erosion. *Int. J. Earth Sci.* 92, 677–690.
- Hourigan, J.K., Reiners, P.W., Brandon, M.T., 2005. U-Th zonation-dependent alpha ejection in (U-Th)/He chronometry. *Geochim. Cosmochim. Acta* 69, 3349–3365.
- Hurford, A.J., 1990. Standardization of fission track dating calibration: recommendations by the Fission Track Working Group of the I.U.G.S. Subcommission on Geochronology. *Chem. Geol.* 80, 171–178.
- Hurford, A.J., Green, P.F., 1983. The zeta age calibration of fission track dating. *Chem. Geol.* 41, 285–312.
- Jahn, A., 1980. Main features of the Tertiary relief of the Sudetes mountains. *Geogr. Pol.* 43, 5–23.
- Janoušek, V., Achler, J., Hanzl, P., Gerdes, A., Erban, V., Žáček, V., Pečina, V., Pudilová, M., Hrdličková, K., Mixa, P., Žáčková, E., 2014. Constraining genesis and geotectonic setting of metavolcanic complexes: a multidisciplinary study of the Devonian Vrbno Group (Hrubý Jeseník Mts., Czech Republic). *Int. J. Earth Sci.* 103 (2), 455–483.
- Jarmołowicz-Szulc, K., 1984. Geochronological study of the northern cover of the Karkonosze granite by fission track method. *Arch. Mineral.* 39, 139–183.
- Jarmołowicz-Szulc, K., Hałas, S., Wojtowicz, A., 2009. Radiometric age analyses of rocks from the northern envelope of the Karkonosze Massif, the Sudetes, Poland: a comparative geochronological study. *Geochronometria* 34, 33–39.
- Jastrzębski, M., Żelaźniewicz, A., Majka, J., Murtezi, M., Bazarnik, J., Kapitonov, I., 2013. Constraints on the Devonian–Carboniferous closure of the Rheic Ocean from a multi-method geochronology study of the Staré Město Belt in the Sudetes (Poland and the Czech Republic). *Lithos* 170, 54–72.
- Jirásek, J., Włosok, J., Sivek, M., Matýsek, D., Schmitz, M., Sýkorová, I., Vašíček, Z., 2014. U-Pb zircon age of the Krásné Loučky tuffite: the dating of Visean flysch in the Moravosilesian Paleozoic Basin (Rhenohercynian Zone, Czech Republic). *Geol. Q.* 58 (4), 659–672.
- Kądziałko-Hofmokl, M., Kruczyk, J., Mazur, S., Siemiątkowski, J., 2003. Paleomagnetism of the upper Proterozoic and Devonian rocks from the Kłodzko Metamorphic Complex in the West Sudetes (SW Poland): tectonic implications for the Variscan belt of Central Europe. *Tectonophysics* 377 (1), 83–99.
- Kądziałko-Hofmokl, M., Szczępański, J., Werner, T., Jeleńska, M., Nejbert, K., 2013. Paleomagnetism and magnetic mineralogy of metabasites and granulites from Orlica-Śnieżnik Dome (Central Sudetes). *Acta Geophys.* 61 (3), 535–568.
- Kalvoda, J., Babek, O., Fatka, J., Leichmann, R., Melichar, S., Nehyba, P., Spacek, 2008. Brunovistulian terrane (Bohemian Massif, Central Europe) from Late Proterozoic to Late Paleozoic: a review. *Int. J. Earth Sci.* 97, 497–518.
- Kasiński, J.R., Panasiuk, M., 1987. Geneza i ewolucja strukturalna niecki żytniawej. *Buletyn Instytutu Geologicznego* 357, 5–35 (in Polish).
- Ketcham, R.A., 2005. Forward and inverse modeling of low-temperature thermochronometry data. *Rev. Mineral. Geochem.* 58, 275–314.
- Ketcham, R.A., Carter, A., Donelick, R.A., Barbarand, J., Hurford, A.J., 2007a. Improved measurement of fission track annealing in apatite using c-axis projection. *Am. Mineral.* 92, 789–798.
- Ketcham, R.A., Carter, A., Donelick, R.A., Barbarand, J., Hurford, A.J., 2007b. Improved modeling of fission track annealing in apatite. *Am. Mineral.* 92, 799–810.
- Kley, J., Voigt, T., 2008. Late Cretaceous intraplate thrusting in central Europe: effect of Africa–Iberia–Europe convergence, not Alpine collision. *Geology* 36, 839–842.
- Kotas, A., Gądecki, S., Buła, Z., Kwarciński, J., Malicki, J., 1983. Geological Atlas of the Upper Silesia Coal Basin, Poland. Part II. Coal Quality Maps (1: 100 000). Geological Institute, Warszawa (In Polish, with English abstract).
- Kowalska, S., Wolański, K., Botor, D., Dunkl, I., Wójtowicz, A., Jonkis, U., Buniak, A., 2015. Complex thermal history reconstruction of Carboniferous rocks from the Fore-Sudetic Monocline – application in a tight gas exploration of illite K-Ar and Zircon helium dating. *EuroClay Conference Abstract Book*, p. 428 Edinburgh, UK, 5–10.07.2015.
- Kříbek, B., Žák, K., Dobeš, P., Leichmann, J., Pudilová, M., René, M., Scharm, B., Scharmová, M., Hájek, A., Holeček, D., Hein, U.F., Lehmann, B., 2009. The Rožná uranium deposit (Bohemian Massif, Czech Republic): shear zone-hosted, late Variscan and post-Variscan hydrothermal mineralization. *Mineral. Deposita* 44, 99–128.
- Kroner, U., Romer, R.L., 2013. Two plates – many subduction zones: the Variscan orogeny reconsidered. *Gondwana Res.* 24, 298–329.
- Kroner, U., Mansy, J.-L., Mazur, S., Aleksandrowski, P., Hann, H.P., Huckriede, H., Lacquement, F., Lamarche, J., Ledru, P., Pharaoh, T.C., Zedler, H., Zeh, A., Zulauf, G., 2008. Variscan tectonics. In: McCann, T. (Ed.), *The Geology of Central Europe*. The Geological Society, London, pp. 599–664.
- Krzywiec, P., 2009. Devonian–Cretaceous repeated subsidence and uplift along the Teisseyre–Tornquist zone in SE Poland – insight from seismic data interpretation. *Tectonophysics* 475 (1), 142–159.
- Kučera, J., Slobodník, M., 2002. Regional extension of hydrothermal veins – result of an important deformation event in the Moravosilesian Paleozoic. *Andean Geol.* 14, 55.
- Kučera, J., Muchez, P., Slobodník, M., Prochaska, W., 2010. Geochemistry of highly saline fluids in siliciclastic sequences: genetic implications for post-Variscan fluid flow in the Moravosilesian Paleozoic of the Czech Republic. *Int. J. Earth Sci.* 99, 269–284.
- Kumpéra, O., 1983. *Geologie spodního karbonu jesenického bloku* (in Czech). Knihovna Ústředního Ústavu Geologického 172 pp. (Praha).
- Kumpéra, O., Martinec, P., 1995. The development of the Carboniferous accretionary wedge in the Moravian–Silesian Paleozoic Basin. *J. Czech Geol. Soc.* 40, 47–64.
- Lange, J.-M., Tonk, C., Wagner, G.A., 2008. Apatite fission track data for the Postvariscan thermotectonic evolution of the Saxon basement – first results. *Z. Dtsch. Ges. Geowiss.* 159, 123–132.
- Lorenz, S., Mroczkowski, J., 1978. The sedimentation and petrography of Zechstein and lowermost Triassic deposits in the vicinity of Kochanów (intra-Sudetic trough). *Geol. Sudet.* 13 (2), 23–39.
- Losert, J., 1957. Deposits and occurrences of lead-zinc ores in the north moravian Culm. *Rozpravy České akademie věd a umění* 67 (4), 1–61.
- Lünen schloss, B., Bayer, U., Muchez, Ph., 1997. Coalification anomalies induced by fluid flow at the Variscan thrust front: a numerical model of the palaeotemperature field. *Geol. Mijnb.* 76, 271–275.
- Malkovský, M., 1987. The Mesozoic and Tertiary basins of the Bohemian Massif and their evolution. *Tectonophysics* 137, 31–42.
- Maluski, H., Rajlich, P., Souček, J., 1995. Pre-Variscan, Variscan and early Alpine thermotectonic history of the north-eastern Bohemian massif: an Ar/Ar study. *Geol. Rundsch.* 84 (2), 345–358.
- Martinek, K., Svojška, M., Filip, J., 2006. Reconstructing post-Carboniferous history of the Krkonoše Piedmont Basin using detrital apatite fission-track data. *Andean Geol.* 20, 91–92.
- Mattern, F., 1995. Late Carboniferous to early Triassic shear sense reversals at strike-slip faults in eastern Bavaria. *Zentralblatt für Geologie und Paläontologie*, Teil I 1471–1490.
- Mazur, S., Aleksandrowski, P., Kryza, R., Oberc-Dziedzic, T., 2006. The Variscan Orogen in Poland. *Geol. Q.* 50, 89–118.
- Mazur, S., Aleksandrowski, P., Turniak, K., Krzeminski, L., Mastalerz, K., Gorecka-Nowak, A., Kurowski, L., Krzywiec, P., Zelazniewicz, A., Fanning, M.C., 2010. Uplift and late orogenic deformation of the Central European Variscan belt as revealed by sediment provenance and structural record in the Carboniferous foreland basin of western Poland. *Int. J. Earth Sci.* 99, 47–64.
- Mazur, S., Szczępański, J., Turniak, K., McNaughton, N.J., 2012. Location of the Rheic suture in the eastern Bohemian Massif: evidence from detrital zircon data. *Terra Nova* 24 (3), 199–206.
- McCann, T., Pascal, C., Timmerman, M.J., Krzywiec, P., Lopez-Gomez, J., Wetzel, A., Krawczyk, C.M., Rieke, H., Lamarche, J., 2006. Post-Variscan (end Carboniferous-Early Permian) basin evolution in Western and Central Europe. In: Gee, D.G., Stephenson, R.A. (Eds.), *European Lithosphere Dynamics*. Geological Society, London, Memoirs Vol. 32, pp. 355–388.
- Migoń, P., Lidmar-Bergström, K., 2001. Weathering mantles and their significance for geomorphological evolution of central and northern Europe since the Mesozoic. *Earth Sci. Rev.* 56, 285–324.
- Milewicz, J., 1997. Góra kreda depresji północnosudeckiej (Ilo-i biostratigrafia, paleogeografia, tektonika oraz uwagi o surowcach) (In Polish). *Acta Universitatis Wratislaviensis, Prace Geologiczno-Mineralogiczne* 61, 1–58.
- Nowak, G., 2003. Petrology of organic matter dispersed in Paleozoic sedimentary rocks of the south-western Poland. *Cuprum* 4 (29), 1–209.
- Rajlich, P., 1990. Strain and tectonic styles related to Variscan transgression and transtension in the Moravo-Silesian Culmian basin, Bohemian Massif, Czechoslovakia. *Tectonophysics* 174 (3–4), 351–367.
- Reicherter, K., Froitzheim, N., Jarosiński, M., Badura, J., Franzke, H.J., Hansen, M., Hübscher, C., Müller, R., Poprawa, P., Reinecker, J., Stachebrandt, W., 2008. Alpine tectonics north of the Alps. In: McCann, T. (Ed.), *The Geology of Central Europe*. Vol. 2. The Geological Society, London, pp. 1233–1285.
- Scheck, M., Bayer, U., Otto, V., Lamarche, J., Banka, D., Pharaoh, T., 2002. The Elbe fault system in North Central Europe – a basement controlled zone of crustal weakness. *Tectonophysics* 360, 281–299.
- Schneider, D.A., Zahner, S.J., Glascock, J.M., Gordon, S.M., Manecki, M., 2006. Thermochronology of the west Sudetes (Bohemian Massif): rapid and repeated education in the eastern Variscides, Poland and Czech Republic. *Am. J. Sci.* 306, 846–873.
- Schulmann, K., Gayer, R., 2000. A model for a continental accretionary wedge developed by oblique collision: the NE Bohemian Massif. *J. Geol. Soc. Lond.* 157, 401–416.
- Schulmann, K., Ledru, P., Autran, A., Melka, R., Lardeaux, J.M., Urban, M., Lobjkowicz, M., 1991. Evolution of nappes in the eastern margin of the Bohemian massif: a kinematic interpretation. *Geol. Rundsch.* 80, 73–92.
- Schulmann, K., Kröner, A., Hegner, E., Wendt, I., Konopásek, J., Lexa, O., Štípková, P., 2005. Chronological constraints on the pre-orogenic history, burial and exhumation of deep-seated rocks along the eastern margin of the Variscan Orogen, Bohemian Massif, Czech Republic. *Am. J. Sci.* 305, 407–448.
- Skoček, V., Valečka, J., 1983. Palaeogeography of the Late Cretaceous quadersandstein of central Europe. *Palaeogeogr. Palaeoclimatol. Palaeoecol.* 44, 71–92.

- Slobodník, M., Muchez, P., Dolníček, Z., 2001. Zn–Pb–Cu mineralization in reef carbonates beneath the Upper Silesian Basin, Czech Republic: possible extremity of the Silesian–Cracow MVT district. *Mineral Deposits at the Beginning of the 21st Century*. AA Balkema, Rotterdam, pp. 209–212.
- Sobczyk, A., Danišík, M., Aleksandrowski, P., Anczkiewicz, A., 2015. Post-Variscan cooling history of the central Western Sudetes (NE Bohemian Massif, Poland) constrained by apatite fission-track and zircon (U–Th)/He thermochronology. *Tectonophysics* 649, 47–57.
- Špacek, P., Kalvoda, J., 2000. Reconstruction of syn-and postsedimentary tectonic events in flysch basin from limestone pebbles variation: Drahany Kulf of the Moravian Rhenohercynian Zone. *Geol. Carpath.* 51 (1), 37–48.
- Špacek, P., Bábek, O., Štepánková, P., Švancara, J., Pazdířková, J., Sedláček, J., 2015. The Nysa–Morava Zone: an active tectonic domain with Late Cenozoic sedimentary grabens in the Western Carpathians foreland (NE Bohemian Massif). *Int. J. Earth Sci.* 104, 963–990.
- Štípká, P., Schulmann, K., 1995. Inverted metamorphic zonation in a basement-derived nappe sequence, eastern margin of the Bohemian Massif. *Geol. J.* 30 (3–4), 385–413.
- Thomson, S.N., 2001. Using apatite fission-track thermochronology to investigate Late Cretaceous tectonic inversion of the Variscan basement blocks of central Germany: examples from the Harz Mountains and Thüringer Wald. *Exkursionsführer und Veröffentlichungen der Deutschen Gesellschaft für Geowissenschaften* 214, 223–224.
- Thomson, S.N., Zeh, A., 2000. Fission-track thermochronology of the Ruhla Crystalline Complex: new constraints on the post-Variscan thermal evolution of the NW Saxonian Massif. *Tectonophysics* 324, 17–35.
- Turniak, K., Mazur, S., Domańska-Siuda, J., Szuszkievicz, A., 2014. SHRIMP U–Pb zircon dating for granitoids from the Strzegom–Sobótka Massif, SW Poland: constraints on the initial time of Permo-Mesozoic lithosphere thinning beneath Central Europe. *Lithos* 208–209, 415–429.
- Uličný, D., 2001. Depositional systems and sequence stratigraphy of coarsegrained deltas in a shallow-marine, strike-slip setting: the Bohemian Cretaceous Basin, Czech Republic. *Sedimentology* 48, 599–628.
- Uličný, D., Špičáková, L., Grygar, R., Svobodová, M., Čech, S., Laurin, J., 2009. Palaeodrainage systems at the basal unconformity of the Bohemian Cretaceous Basin: roles of inherited fault systems and basement lithology during the onset of basin filling. *Bull. Geosci.* 84 (4), 577–610.
- Ulrych, J., Dostál, J., Adamovic, J., Jelínek, E., Špacek, P., Hegner, E., Balogh, K., 2011. Recurrent Cenozoic volcanic activity in the Bohemian Massif (Czech Republic). *Lithos* 123, 133–144.
- Unrug, R., 1977. Lower Carboniferous Flysch in the Głubczyce region (in Polish with English summary). *Roczn. Pol. Towarz. Geol.* 47, 72–99.
- Unrug, R., Dembowksi, Z., 1971. Diastrophic and sedimentary evolution of the Moravia–Silesia Basin (in Polish with English summary). *Roczn. Pol. Towarz. Geol.* 41, 118–168.
- Vamvaka, A., Siebel, W., Chen, F., Rohrmuller, J., 2014. Apatite fission-track dating and low-temperature history of the Bavarian Forest (southern Bohemian Massif). *Int. J. Earth Sci.* 103, 103–119.
- Ventura, B., Lisker, F., 2003. Long-term landscape evolution of the northeastern margin of the Bohemian Massif: apatite fission-track data from the Erzgebirge (Germany). *Int. J. Earth Sci.* 92, 691–700.
- Ventura, B., Lisker, F., Kopp, J., 2009. Thermal and denudation history of the Lusatian Block (NE Bohemian Massif, Germany) as indicated by apatite fission-track data. In: Lisker, F., Ventura, B., Glasmacher, U.A. (Eds.), *Thermochronological Methods: From Palaeotemperature Constraints to Landscape Evolution Models*. Geological Society, London, Special Publications Vol. 324, pp. 181–192.
- Voigt, T., 2009. The Lusatia–Krkonoše high as a late Cretaceous inversion structure: evidence from the surrounding Cretaceous basins. *Z. Geol. Wiss.* 37, 15–39.
- Wagner, G.A., Coyle, D.A., Duyster, J., Henjes-Kunst, F., Peterek, A., Schröder, B., Stöckhert, B., Wemmer, K., Zulauf, G., Ahrendt, H., Bischoff, R., Hejl, E., Jacobs, J., Menzel, D., Van den Haute, P., Vercoutere, C., Welzel, B., 1997. Post-Variscan thermal and tectonic evolution of the KTB site and its surroundings. *J. Geophys. Res.* 102, 18221–18231.
- Wilson, M., Neumann, E.R., Davies, G.R., Timmerman, M.J., Heeremans, M., Larsen, B.T., 2004. Permo-Carboniferous magmatism and rifting in Europe: introduction. In: Wilson, M., Neumann, E.-R., Davies, G.R., Timmerman, M.J., Heeremans, M., Larsen, B.T. (Eds.), *Permo-Carboniferous Magmatism and Rifting in Europe*. Geological Society, London, Special Publications 223(1), pp. 1–10.
- Wojewoda, J., 1997. Upper Cretaceous littoral-to-shelf succession in the Intrasudetic Basin and Nysa trough, Sudety Mts (in Polish with English summary). In: Wojewoda, J. (Ed.), *Obszary źródłowe: zapis w osadach*. Vol. 1, pp. 81–96.
- Wojewoda, J., Rauch, M., Kowalski, A., 2016. Synsedimentary seismotectonic features in Triassic and Cretaceous sediments of the Intrasudetic Basin (U Deviti Křížů locality) – regional implications. *Geol. Q.* 60 (2), 355–364.
- Wolff, R., Dunkl, I., Lange, J.-M., Tonk, C., Voigt, T., von Eynatten, H., 2015. Superposition of burial and hydrothermal events: post-Variscan thermal evolution of the Erzgebirge, Germany. *Terra Nova* 27, 292–299.
- Zapletal, J., Dvořák, J., Kumpera, O., 1989. Stratigraphical classification of the Culm of the Nízký Jeseník Mts. (in Czech). *Věstník Ústředního Ústavu Geologického* 64, 243–250.
- Ziegler, P.A., 1987. Late Cretaceous and Cenozoic intraplate compressional deformations in the Alpine foreland. *Tectonophysics* 137, 389–420.
- Ziegler, P.A., Dézes, P., 2007. Cenozoic uplift of Variscan Massifs in the Alpine foreland: timing and controlling mechanisms. *Glob. Planet. Change* 58, 237–269.
- Ziegler, P.A., Bertotti, G., Cloetingh, S., 2002. Dynamic processes controlling foreland development: the role of mechanical (de)coupling of orogenic wedges and forelands. In: Bertotti, G., Schulmann, K., Cloetingh, S. (Eds.), *Continental Collision and the Tectono-Sedimentary Evolution of Forelands*. Europ. Geophys. Soc. Stephan Mueller Special Publication Series vol. 1, pp. 29–91.
- Zimák, J., Losos, Z., Novotný, P., Dobes, P., Hladíková, J., 2002. Study of vein carbonates and notes to the genesis of the hydrothermal mineralization in the Moravo–Silesian Culm. *J. Czech Geol. Soc.* 47, 111–122.